A roadmap to estimating agricultural ammonia volatilization over Europe using satellite observations and simulation data

Rimal Abeed[1], Camille Viatte[1], William C. Porter[2], Nikolaos Evangeliou[3], Cathy Clerbaux[1,4], Lieven Clarisse[4], Martin Van Damme[4,5], Pierre-François Coheur[4], and Sarah Safieddine[1]

[1]LATMOS/IPSL, Sorbonne Université, UVSQ, CNRS, Paris, France
[2]Department of Environmental Sciences, University of California, Riverside, CA 92521, USA
[3]Norwegian Institute for Air Research (NILU), Department of Atmospheric and Climate Research (ATMOS), Kjeller, Norway
[4]Université libre de Bruxelles (ULB), Spectroscopy, Quantum Chemistry and Atmospheric Remote Sensing (SQUARES), Brussels, Belgium
[5]Belgian Institute for Space Aeronomy (BIRA-IASB), Brussels 1180, Belgium

Correspondence to: Rimal Abeed rimal.abeed@latmos.ipsl.fr

Abstract

Ammonia (NH_3) is one of the most important gases emitted from agricultural practices. It affects air quality and the overall climate, and in turn influenced by long term climate trends as well as by short term fluctuations in local and regional meteorology. Previous studies have established the capability of the Infrared Atmospheric Sounding Interferometer (IASI) series of instruments aboard the Metop satellites to measure ammonia from space since 2007. In this study, we explore the interactions between atmospheric ammonia, land and meteorological variability, and long-term climate trends in Europe. We investigate the emission potential (Γ_{soil}) of ammonia from the soil, which describes the soil – atmosphere ammonia exchange. Γ_{soil} is generally calculated in-field or in laboratory experiments; here, and for the first time, we investigate a method which assesses it remotely using satellite data, reanalysis data products, and model simulations.

We focus on ammonia emission potential during March 2011, which marks the start of growing season in Europe. Our results show that Γ_{soil} ranges from 2×10^3 to 9.5×10^4 (dimensionless) in a fertilized cropland, such as in the North European Plain, and is of the order of $10 - 10^2$ in a non-fertilized soil (e.g. forest and grassland). These results agree with in-field measurements from the literature, suggesting that our method can be used in other seasons and regions in the world. However, some improvements are needed in the determination of mass transfer coefficient k (m s^{-1}), which is a crucial parameter to derive Γ_{soil}.

Using a climate model, we estimate the expected increase in ammonia columns by the end of the century based on the increase in skin temperature (T skin), under two different climate scenarios. Ammonia columns are projected to increase by up to 50 %, particularly in Eastern Europe, under the SSP2-4.5 scenario, and might even double (increase of 100 %) under the SSP5-8.5 scenario. The increase in skin temperature is responsible for a formation of new hotspots of ammonia in Belarus, Ukraine, Hungary, Moldova, parts of Romania, and Switzerland.

1. Introduction

51

Ammonia (NH₃) emissions have been increasing in a continuous manner from 1970 to 2017 (McDuffie et al., 2020). During the period 2008 – 2018 alone, the increase in ammonia columns in Western and Southern Europe amounted to 20.8 % yr^{-1} ($\pm$ 4.3 %), and to 12.8 ($\pm$ 1.3 %) globally (Van Damme et al., 2021). Although ammonia alone is stable against heat and light, it is considered a very reactive base, and it constitutes the largest portion of the reactive nitrogen (N_r) on Earth. The vast majority of atmospheric ammonia not deposited is transformed into fine particulate matter (PM$_{2.5}$) composed of ammonium (NH$_4^+$), through acid – base chemical reactions with available acids in the environment, namely sulfuric acid (H$_2$SO$_4$), hydrochloric acid (HCl), and nitric acid (HNO$_3$) (Yu et al., 2018), while only 10 % of the total ammonia gas is believed to be oxidized by hydroxyl radicals (OH$^-$) (Roelle and Aneja, 2005). PM$_{2.5}$ has degrading effects on human health, especially respiratory diseases (Bauer et al., 2016). Soils are known to be a source of atmospheric ammonia, especially in areas of intensive agricultural practices (Schlesinger and Hartley, 1992), and this is due to enriching the soil with the reactive nitrogen present in fertilizers. The increase in the application of synthetic fertilizers, and intensification of agricultural practices is believed to be the dominant factor of the global increase in ammonia emissions over the past century (Behera et al., 2013; McDuffie et al., 2020). In addition to agriculture, ammonia can be emitted from industrial processes, biomass burning (Van Damme et al., 2018), and natural sources such as from seal colonies (Theobald et al., 2006).

Following the application of fertilizers, ammonium and ammonia are released in the soil. Prior to its volatilization, ammonia in the soil exists either in the gas phase (NH$_{3\,(g)}$) or in the aqueous/liquid phase (NH$_{3\,(aq)}$), the equilibrium between both states of ammonia is governed by Henry's law (Wentworth et al., 2014), as shown in the Appendix. The dissociation of ammonia in soil water is a function of soil acidity (pH) and temperature (Roelle and Aneja, 2005) (Eq. (A-1) and (A-2) in Appendix A), and controlled by the dissociation constant $K_{NH_4^+}$. Once released to the atmosphere, ammonia near the surface exists is in the gas phase, hence Henry's law can be used to describe the equilibrium between ammonia in the soil (liquid phase), and near the surface (gas phase). This bi-directional exchange between the soil and the atmosphere will continue until the equilibrium is reached, and this occurs when ammonia concentration is equal to the compensation point χ_{NH_3} (the concentration of ammonia at equilibrium). The flux of ammonia from the soil to the atmosphere (emission) occurs when the concentration of atmospheric ammonia is less than the compensation point χ_{NH_3}, while ammonia deposition occurs when the concentration of ammonia is equal to or greater than χ_{NH_3} (Flechard et al., 2011; Wichink Kruit, 2010). It is then crucial to quantify the compensation point in order to understand this bi-directional exchange. The main variables needed to calculate χ_{NH_3} are soil temperature (T skin) and Γ_{soil}, which is a dimensionless ratio between ammonium and pH (NH$_4^+{}_{(aq)}$ and H$^+{}_{(aq)}$ concentrations, respectively, in the soil). All the equations are described in Appendix A (Eq. (A-1) to (A-15)).

The soil emission potential (Γ_{soil}) has been thoroughly investigated in field and controlled laboratory environments (e.g. David et al., 2009; Flechard et al., 2013; Massad et al., 2010; Mattsson et al., 2008; Nemitz et al., 2000; Wentworth et al., 2014, among others). Γ_{soil} is dimensionless and it can range from 20 (non-fertilized soil in a forest) to the order of 10^6 (mixture of slurry in a cropland). It is found to peak right after fertilizers application, due to the increase in ammonium content in the soil (a product of urea hydrolysis), and to return to pre-fertilization levels 10 days after the application (Flechard et al., 2010; Massad et al., 2010). Little information exists on regional or global scales to assess the large-scale spatial variability of ammonia emission potentials.

In order to meet the needs of a growing population, agricultural practices have intensified during the 2003 – 2019 period (more fertilizer use per surface area), resulting in increased net primary production (NPP) per capita (Potapov et al., 2022) and volatized ammonia (due to increase in both nitrogen soil content, and cultivated lands). In Europe alone, the area of croplands increased by 9 % from 2003 to 2019, and most of the expansion took place on lands that were abandoned for more than 4 years (Potapov et al., 2022). Around 90 % of the mineral fertilizers used in Europe are nitrogen-based, with urea and nitrate fertilizers dominating the market in the 27 EU countries, since they make up 22 % and 45 % of the total market (Fertilizers Europe, 2016). With the increase in croplands area and agricultural activities, climate change will have a significant effect on agricultural practices, with warmer climates enhancing the volatilization of ammonia from soils, especially in intensely fertilized lands (Shen et al., 2020).

This study aims at exploring ammonia emission potential and volatilization in Europe, using infrared satellite data of ammonia columns, reanalysis temperature data, and chemical transport model simulations to provide information on chemical sources and sinks. We specifically study the relationship between satellite-derived ammonia concentration at the start of the growing

103 season, soil emission potentials and their spatial variability over Europe during March of 2011. Section 2 provides the
104 methods/datasets used. The results are described in Sect.3, including simulation from GEOS-Chem in Sect. 3.1. Regional
105 emission potentials are shown and discussed in Sect. 3.2. Using a climate model, future projections of ammonia columns are
106 investigated under different climate scenarios in Sect. 3.3. Conclusions are listed in Sect. 4.

2. Methodology

2.1. Calculation of the emission potential

110 In this study, we use IASI satellite data to calculate the ammonia emission potential Γ_{soil} instead of field soil measurements. In
111 field studies, Γ_{soil} is calculated by measuring the concentration of ammonium (NH_4^+) and H^+ (10^{-pH}) in the soil; the ratio
112 between both of these concentrations is Γ_{soil}. Here, we use infrared satellite observations which offer a regional coverage over
113 Europe. With these, however, we cannot monitor soil content of ammonium nor its pH. This renders the remote Γ_{soil} calculation
114 challenging, and less straight forward. The full derivation of the equation used to calculate the emission potential is explained
115 in Appendix A. In short, upon its dissolution in the soil water, ammonia follows Henry's law. In steady state conditions between
116 the soil and the near surface, the amount of the ammonia emitted and lost is considered equal. Based on this assumption, the
117 soil emission potential (dimensionless) is calculated as follows Eq. (2-1) or Eq. (A-15) in Appendix A:
118

$$\Gamma_{soil} = \frac{[NH_3]^{col} \cdot T_{soil}}{\exp(\frac{-b}{T_{soil}})} \frac{M_{NH_3}}{a \cdot N_a \cdot c'} \cdot \frac{1}{k\tau} \tag{2-1}$$

119
120 where $[NH_3]^{col}$ is the total column concentration of ammonia (molecules cm⁻²), measured by satellite remote sensors, T_{soil} is
121 the soil temperature at the surface, which can be expressed as the skin temperature, T skin (Kelvin), a and b are constants ($a =$
122 $2.75 \times 10^3 \; g \; K \; cm^{-3}$, $b = 1.04 \times 10^4 \; K$), M_{NH_3} is the molar mass of ammonia ($M = 17.031 \; g \; mol^{-1}$), and N_a is
123 Avogadro's number ($N_a = 6.0221409 \times 10^{23} \; molecules \; mol^{-1}$), c' is 100 and is added to convert k from m s⁻¹ to cm s⁻¹
124 (since $[NH_3]^{col}$ is in molecules cm⁻²), and τ the lifetime of ammonia (seconds).
125 k is the soil – atmosphere exchange coefficient or deposition velocity (cm s⁻¹), also known as the mass transfer coefficient (this
126 nomenclature will be used in this study). It is a function of the roughness length of the surface, wind speed, the boundary layer
127 height (Olesen and Sommer, 1993; Van Der Molen et al., 1990), and pH (Lee et al., 2020). It can also be calculated using a
128 resistance model, often used to explain the exchange between the surface and the atmosphere (Wentworth et al., 2014).
129 Different studies provide look up tables values of k for different land cover types and different seasons based on this resistance
130 model (Aneja et al., 1986; Erisman et al., 1994; Phillips et al., 2004; Roelle and Aneja, 2005; Svensson and Ferm, 1993; Wesely,
131 1989).
132 In general, the mass transfer coefficient k is in the order of 10^{-3} to 10^{-2} m s⁻¹ in a mixture of soil and manure, and 10^{-6} to 10^{-5} m
133 s⁻¹ in a mixture of manure alone (Roelle and Aneja, 2005). We discuss and provide more information on k in Sect. 3.2, and
134 additional details on this calculation in general are provided in Appendix A.
135

2.2. IASI ammonia, ERA5 T skin, and MODIS Land cover

137
138 The Infrared Atmospheric Sounding Interferometer (IASI) is considered the most innovative instrument onboard the
139 polar-orbiting Metop satellites (Klaes, 2018). Three IASI instruments are onboard Metop-A, B and C, the series of satellites
140 launched by the EUMETSAT (European Organization for the Exploitation of Meteorological Satellites) in 2006, 2012, and
141 2018, respectively. The Metop-A satellite was de-orbited in October 2021 (Lentze, 2021), and as a result only two instruments
142 (IASI-B and C onboard Metop-B and C) are operating today. The observations from IASI cover any location on Earth at 9:30
143 in the morning (AM) and in the evening (PM), local solar time. It can detect a variety of atmospheric species including trace
144 gases (Clerbaux et al., 2009). The IASI Fourier-transform spectrometer monitors the atmosphere in the spectral range between
145 645 and 2760 cm⁻¹ (thermal infrared), and is nadir-looking. IASI has a swath width that measures 2200 km, with a pixel size
146 of ~12 km.
147
148 Ammonia was first detected with IASI using the υ_2 vibrational band of ammonia (~950 cm⁻¹) (Clerbaux et al., 2009; Coheur et
149 al., 2009). The ammonia total columns used in this study are the product of an Artificial Neural Network and re-analyzed
150 temperature data from the European Centre for Medium-Range Weather Forecasts (ECMWF) product ERA5 ANNI-NH₃-v3R-

151 ERA5 (Van Damme et al., 2021). Several studies used ammonia data from IASI to study hotspots of ammonia of different
152 source types including both natural and anthropogenic sources (Clarisse, Van Damme, Clerbaux, et al., 2019; Clarisse, Van
153 Damme, Gardner, et al., 2019; Dammers et al., 2019; Van Damme et al., 2018, 2021; Viatte et al., 2021). Recently, IASI
154 observations were used to study the effect of war and conflict on agricultural practices in Syria (Abeed et al., 2021).
155
156 Fewer errors on the retrieval were observed during the day and over land (Van Damme et al., 2017), hence, we use only daytime
157 ammonia measurements from IASI. Comparisons with ammonia measured using a ground-based instrument showed a good
158 correlation of R=0.75 (Viatte et al., 2021). Satellite ammonia data from CrIS (Crosstrack Infrared Sounder) (Shephard and
159 Cady-Pereira, 2015) were compared with those from IASI, and were equally found to give similar results when looking at
160 concentrations from a wildfire (Adams et al., 2019), showing consistency when studying seasonal and inter-annual variability
161 (Viatte et al., 2020).
162
163 In addition to ammonia, we look at skin temperature (T skin or land surface temperature LST) data from the ECMWF reanalysis
164 (ERA5) at a grid resolution of 0.25×0.25 ° (Hersbach et al., 2020). ERA5 Temperatures are interpolated temporally and
165 spatially to the IASI morning overpass (~9:30 A.M. local time), since we only consider daytime ammonia. ERA5 temperature
166 data are also used in the retrieval process of the ammonia data we used in this study NH_3-v3R-ERA5 (Van Damme et al., 2021).
167 T skin is defined as the temperature of the uppermost surface layer when radiative equilibrium is reached. It also represents the
168 theoretical temperature required in order to reach the surface energy balance (ECMWF, 2016). Skin temperature in Europe
169 varies with a standard deviation on the daily average that is mostly between 2 and 6°C, in Northern, Central, Western and
170 South-western Europe. And between 4 to 8°C in Eastern Europe (not shown here).
171
172 In order to assign a mass transfer coefficient k to each land type, the moderate resolution imaging spectroradiometer (MODIS),
173 a series of instruments orbiting the Earth aboard the Aqua and Terra satellites, is used. The data product MCD12Q1 (version
174 6) is a combined Aqua/Terra Land cover type product, with a spatial resolution of 500 m. This product provides maps of land
175 cover type from 2001 through 2019 (Sulla-Menashe and Friedl, 2018). From the land use categories included in the MOD12Q1
176 product (Belward et al., 1999) we focus on croplands, forests, shrublands, and grasslands. We do not include barelands, snow
177 cover, and urban areas in our analysis; we are not interested in studying these surfaces, since we focus on ammonia volatilization
178 from the soil in areas where fertilizers are applied. In addition to croplands, in this study we show the emission potential in
179 forests and grasslands/shrublands for comparison with values in the literature. In an attempt to calculate an emission potential
180 (Eq. (2-1)) that is relevant to the land cover/use, we therefore assign a mass transfer coefficient k to each land type based on
181 literature values (Aneja et al., 1986; Erisman et al., 1994; Roelle and Aneja, 2005; Svensson and Ferm, 1993; Wesely, 1989)
182 and we discuss it in Sect. 3.2.
183

184 **2.3. Model simulations**

185   2.3.1. **GEOS-Chem Chemistry Transport Model**

186
187 In this study we use version 12.7.2 of the GEOS-Chem chemical transport model (Bey et al., 2001). The model is driven by
188 the Modern-Era Retrospective Analysis for Research and Applications version 2 (MERRA-2) reanalysis product, including
189 nested domains over Europe at a $0.5° \times 0.625°$ horizontal resolution. MERRA-2 is the second version of the MERRA
190 atmospheric reanalysis product by NASA Global Modulation Assimilation Office (NASA/GMAO) (Gelaro et al., 2017).
191 Boundary conditions for the nested domains are created using a global simulation for the same months at $2° \times 2.5°$ resolution.
192 We generate model output for March of 2011, preceded by a one month of discarded model spin-up time for the nested run,
193 and two months for the global simulation. March corresponds well to the beginning of the growing season (FAO, 2022; USDA,
194 2022), and as such to the month of fertilizers application in Europe.
195
196 Output includes the hourly mean for selected diagnostics. Anthropogenic emissions are taken primarily from the global
197 Community Emissions Data System (CEDS) inventory (Hoesly et al., 2018). Biogenic non-agricultural ammonia, as well as
198 ocean ammonia sources, are taken from the Global Emission Inventories Activities database (GEIA, (Bouwman et al., 1997)).
199 Open fire emissions are generated using the GFED 4.1s inventory (Randerson et al., 2015). We used the Harmonized Emissions
200 Component module (HEMCO) to obtain the ammonia emissions over Europe (Keller et al., 2014).
201

202   2.3.2. **EC-Earth Climate model**

203   To analyze how future climate will affect ammonia concentration and emission potential, we use the ECMWF European Earth
204   Consortium climate model (EC-Earth, http://www.ec-earth.org/). While other climate models exist, we choose this one because
205   the ammonia product from IASI uses ERA5 for the retrievals and we calculate the emission potential from the T skin product
206   of ERA5. The reanalysis uses the ECMWF Integrated Forecasting System for the atmosphere–land component (IFS). IFS is
207   also used in EC-Earth and is complemented with other model components to simulate the full range of Earth system interactions
208   that are relevant to climate (Döscher et al., 2021). We note that the versions of the IFS models used in ERA5 and in EC-Earth
209   are not identical as the climate model product is not assimilated and is not initialized with observations several times a day like
210   ERA5. The EC-Earth simulations are included in the Climate model intercomparison project, phase 6 (Eyring et al., 2016), part
211   of the Intergovernmental Panel on Climate Change (IPCC) report of 2021 (Masson-Delmotte, et al., 2021). We use the so-
212   called Scenario Model Intercomparison Project (ScenarioMIP), covering the period [2015 – 2100] for future projections under
213   different shared socio-economic pathways (SSP) (Riahi et al., 2017). We analyze two scenarios: the SSPP2-4.5, a "middle of
214   the road" socio-economic scenario with a nominal 4.5 W/m^2 radiative forcing level by 2100, similar to the RCP-4.5 scenario,
215   and the SSP5-8.5, the upper edge of the SSP scenario spectrum with a high fossil-fuel development use over the 21st century.

216   **2.4. GEOS-Chem validation with IASI**

217
218   To analyse how well the model simulates atmospheric ammonia, we compare the simulated GEOS-Chem hourly averaged
219   (March 2011) ammonia total columns output (Sect. 2.3.1) with the IASI-NH$_3$ total columns gridded on the same horizontal
220   resolution ($0.5° \times 0.625°$) and during the same month. We applied temporal coincidence criterion to GEOS-Chem outputs in
221   order to compare them with IASI morning observations. For instance, we selected data between 8:30 and 11:30 UTC in the
222   GEOS-Chem model output.
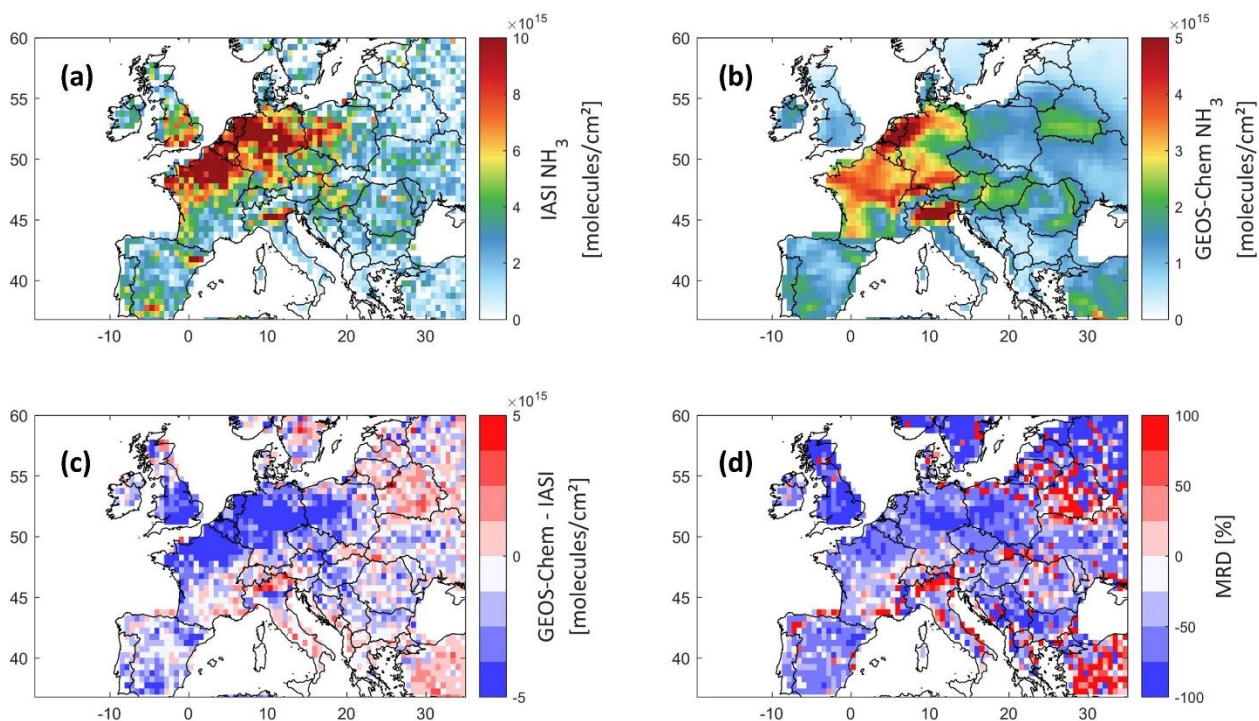
Figure 1. Ammonia total column concentrations from IASI (panel a), and GEOS-Chem (panel b), the difference between both datasets (panel c) in molecules cm^{-2}, and the Mean Relative Difference (MRD) in % (panel d); all data are a monthly average of March 2011, and over Europe at a $0.5° \times 0.625°$ grid resolution. Note that the colour bar limits are different between panels (a) and (b).

223

224

225 Figure 1shows the IASI NH$_3$ distribution (Figure 1a), and that from GEOS-Chem (Figure 1b), the bias between the two (Figure
226 1c), and the mean relative difference MRD (Figure 1d), all during March 2011. MRD is calculated as the mean of the ratio
227 $\frac{(GeosChem\ NH_3 - IASI\ NH_3) \times 100}{IASI\ NH_3}$ at each grid point.

228

229

230 Generally, both GEOS-Chem and IASI show coincident sources of ammonia, reflecting the good ability of the model to
231 reproduce ammonia columns over major agricultural source regions in Europe. The bias between IASI and GEOS-Chem and
232 the mean relative difference (MRD) are shown in Figure 1c and d. Ammonia columns from GEOS-Chem are underestimated
233 by up to 2×10^{16} molecules/cm² in some source regions/hotspots, especially in England, North Eastern France, the North
234 European Plain (Netherlands, Belgium), and Spain (around Barcelona). Similar results were found in the study of Whitburn et
235 al. (2016), in which they show that GEOS-Chem underestimates ammonia columns by up to 1×10^{16} molecules/cm² in Europe
236 on a yearly average in 2009, notably in the North European Plain. It is important to note that, in our study, we compare only
237 one month of data (March, 2011) which marks the start of the growing season in the majority of the countries of interest (FAO,
238 2022; USDA, 2022). The differences are most likely due to the fact that, with IASI, cloud-free data are used to retrieve
239 ammonia. In most of the studied regions, the MRD is around 50 % (±7 %) in absolute value, for instance, in Brittany MRD =
240 −43 %, whereas in both Barcelona and Valladolid in Spain, it is −57 %. While England shows the highest MRD value in
241 absolute terms (−79 %), the best represented region is the Po Valley (+0.1 %), then follows the region of New Aquitaine in
242 the southwest of France (−34.1 %) (see Table 1). A summary of the results of this study, including the MRD over some source
243 regions is listed in Table 1. Although the biases and MRD values can be considered as high, the spatial distribution is consistent
244 between IASI and GEOS-Chem. Therefore, we assume that meteorological and soil parameters affecting one dataset (e.g. IASI
245 NH$_3$) are applicable to the other (e.g. model simulation), this is known as the steady-state approximation. It is worth noting that

246 although we do not use the latest version of GEOS-Chem, the results we obtain reflect our current understanding of the regional
247 chemistry at this horizontal and temporal resolution.
248
249 The frequency of fertilizers application can vary per crop type and per country, as well as from year to year. In Europe, however,
250 the N applied per surface area is quite stabilized after year 1980, with some interannual fluctuations in most European countries
251 (Einarsson et al., 2021). As to our knowledge, accurate information on the application frequency per country is not reported.
252 While the application frequency can change from year to year, the fluctuations are less pronounced after the year 2000. For
253 instance, in France and Belgium the nitrogen content fluctuates between 100 and 110 kg N/ha/year, from 2000 to 2020
254 (Einarsson et al., 2021).
255

3.   Results and discussions

3.1.   Ammonia emissions, losses and lifetime in Europe

258 In order to understand the NH_3 spatial variability in Europe during the application of fertilizers, a detailed analysis of the output
259 of the GEOS-Chem simulation for the month of March 2011 is shown in Figure 2.
260 The anthropogenic sources (i.e. mainly agriculture) contribute 83 % of the total ammonia emissions during March 2011 in
261 Europe. The ammonia emissions from natural sources (i.e. soil of natural vegetation, oceans, and wild animals) follow
262 representing 16 % of the total emissions, whereas the remaining 1 % correspond to the ammonia emissions from biomass
263 burning and ships (not shown here).
264 Figure 2a shows the monthly emissions of ammonia. Most of these emissions are due to agricultural activities (not shown here);
265 we identify 8 source regions which we investigate thoroughly in this study shown as rectangles A to H. The highest agricultural
266 sources over Europe include the North European Plain, Brittany, and the Po Valley (regions C, D, and F).
267 In the calculation of the total loss of ammonia (Figure 2b), we considered dry deposition, chemistry, transport, and wet
268 deposition (in which we included ammonia loss to convection) from the GEOS-Chem model simulation, which are all possible
269 loss processes for ammonia (David et al., 2009). Figure 2b shows that the largest losses occur logically where we have the
270 highest sources detected (see Figure 2a).
271
272
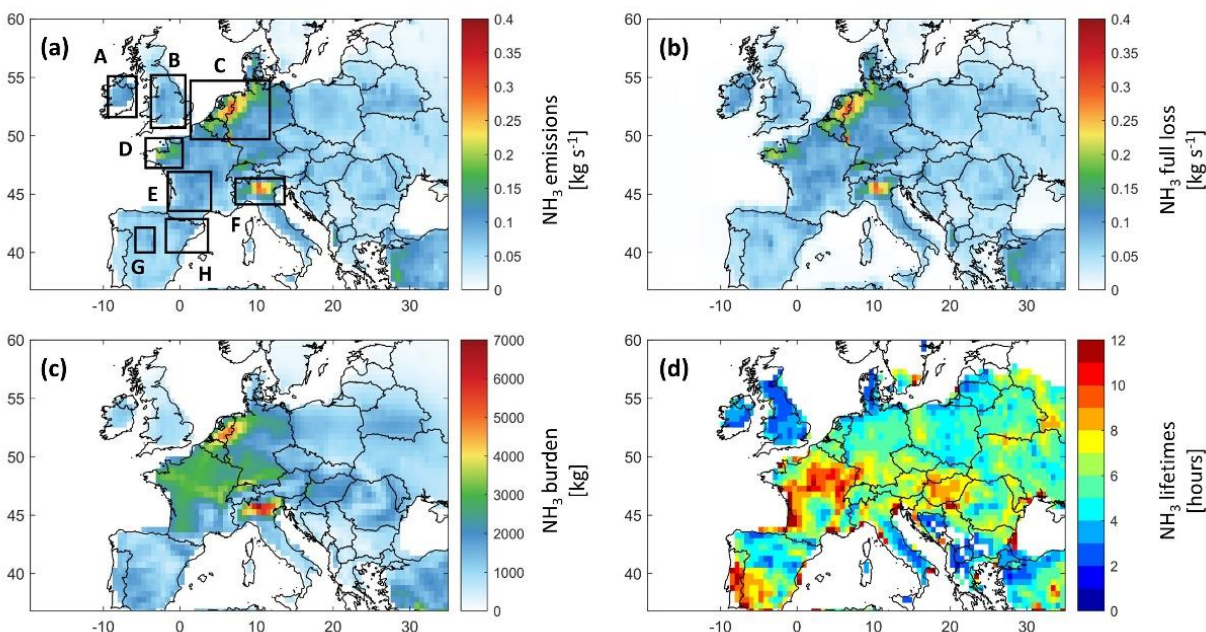
Figure 2. Ammonia budget in Europe from GEOS-Chem: (a) Ammonia emissions from the Harmonized Emissions Component module (HEMCO) in kg s⁻¹ with our regions of interest shown in rectangles, (b) ammonia full loss in kg s⁻¹, (c) ammonia total burden in kg, and (d) ammonia lifetime in hours. All plots refer to March 2011 and are presented at a $0.5° \times 0.625°$ grid resolution.

273 The total ammonia burden (Figure 2c) is calculated as the integrated sum of all ammonia columns in the model grid box. We
274 can clearly detect ammonia hotspots over Europe, in particular the North European Plain, Brittany and the Po Valley, all regions
275 characterized by intense agricultural activities, as the total emissions and deposition show (Figure 1and Figure 2). We also see
276 that the burden is generally the highest over France, Belgium, The Netherlands, and parts of Germany and Italy.
277
278 The lifetime τ_{ss} of ammonia is shown in Figure 2d. In the case of a gas with a short lifetime, such as ammonia, the emissions
279 are relatively well-balanced spatially by eventual sinks/losses (steady-state approximation). Therefore, we can calculate a
280 steady-state lifetime as the ratio between the total burden B (Figure 2c) and the total emissions E or losses L (sum of all emitted
281 / lost molecules, Figure 2a or b) using the following equation: $\tau_{ss} = {B}/{L}$ (Plumb and Stolarski, 2013).
282
283 We note that the τ_{ss} is more or less the same whether we calculate it using the losses or the emissions. For instance, in selected
284 source regions (rectangles in Figure 2a) the total emissions and losses are very close with very low biases that are less than 2%
285 (not shown here). Our results show that τ_{ss}, on a monthly average, can go up to 12 hours, and it can reach 1 day (24 hours) in
286 coastal regions such as region E in New Aquitaine in France. The latter can be related to the high probability of air stagnation
287 in that area, especially during spring, in comparison to Northern Europe (Garrido-Perez et al., 2018), since higher PM$_{2.5}$
288 pollution episodes were found under stagnant meteorological conditions (AQEG, 2012), and these PM$_{2.5}$ particles can
289 dissociate, releasing ammonia. Our results agree with the literature suggesting a residence time between a few hours to a few
290 days (Behera et al., 2013; Pinder et al., 2008). We note that Evangeliou et al. (2021) estimated the lifetime of ammonia over
291 Europe using a different model and the results showed a monthly average ranging from 10 to 13 hours. The figure adapted from
292 Evangeliou et al. (2021) is shown in supplementary material (Figure S1). Shorter lifetimes from industrial sources of ammonia
293 were reported in Dammers et al. (2019), with a mean lifetime of ammonia that is equal to 2.35 hours (±1.16). A recent study
294 found lifetimes of ammonia that vary between 5 and 25 hours, roughly, in Europe (Luo et al., 2022); these values are higher
295 since, in addition to ammonia loss, Luo et al. (2022) included the loss of ammonium, and thus considered the loss of ammonia
296 only terminal when the ammonium is also lost/deposited. This approach is not adopted here nor in Evangeliou et al. (2021).
297
298 Notably, ammonia lifetime and burden (Figure 2c, and d) each have different spatial distribution compared to the other 2 panels
299 (Figure 2a, and b). The ammonia residence time in the atmosphere varies depending on the sources and more importantly on
300 the locally dominant loss mechanisms. For this reason, in Figure 3, we show the relative contribution of the ammonia loss
301 mechanisms, presented as pie charts, for the agricultural source regions shown in black boxes in Figure 2a.
302

303 The fastest loss mechanisms are either chemical (i.e. in the vast majority transformation to particulate matter) or through wet
304 and dry deposition (Tournadre et al., 2020). Figure 3 shows that more than 50 % of the ammonia molecules in the atmosphere
305 are lost to chemical reactions in most of the regions (A, B, C, H, and F). The shortest residence time of ammonia is observed
306 in England, where the chemical removal was significantly higher than other sinks and represented up to 73 % of the total
307 ammonia loss pathways, suggesting a rapid transformation into inorganic particulate matter ($PM_{2.5}$). In the regions D, G and E
308 the chemical loss makes up 50 %, 49 %, and 42 %, respectively. In fact, in March 2011, PM was found to be mostly composed
309 of inorganic nitrate (41 %), and ammonium (20 %) (Viatte et al., 2022) over Europe, both of which are products of atmospheric
310 ammonia. Nitrate-bearing $PM_{2.5}$ are formed when nitric acid (HNO_3) reacts with ammonia (Yang et al., 2022), and ammonium
311 is a direct product of the hydrolysis of ammonia. 41% of the nitric acid formed in the atmosphere is produced from the reaction
312 between nitrogen dioxide (NO_2) and the hydroxyl radical (OH) (Alexander et al., 2020). These chemical pathways help explain
313 the large chemical losses in most of the regions studied in Figure 3.
314
315 Ammonia loss to transport is the highest in regions neighbouring the Atlantic Ocean, accounting for 30 %, 27 %, 32 %, and 34
316 % of total sinks in regions A, D, E, and G respectively. These regions are exposed to the North Atlantic Drift, also known as
317 the Gulf Stream, that is associated with high wind speed and cyclonic activity (Barnes et al., 2022). Although the gulf stream
318 also affects the loss to transport in England (region B), the chemical loss is the dominant one. Acids, such as HNO_3 and H_2SO_4
319 react with ammonia in the atmosphere. Therefore, high atmospheric concentrations of NO_2 and SO_2 (from which HNO_3 and
320 H_2SO_4 are derived respectively), induce higher loss of ammonia to chemical reactions. In England, the annual concentration
321 mean of both NO_2 and SO_2 are higher than in Ireland (European Environment Agency, 2017a, 2017b). This can explain why
322 the largest proportion of NH_3 is lost to chemistry in England, in spite of the effect of the gulf stream. In other regions, 14 % to
323 22 % of the total ammonia is lost to transport mechanisms, and in all regions, 11 to 22 % is lost to dry deposition (Figure 3).
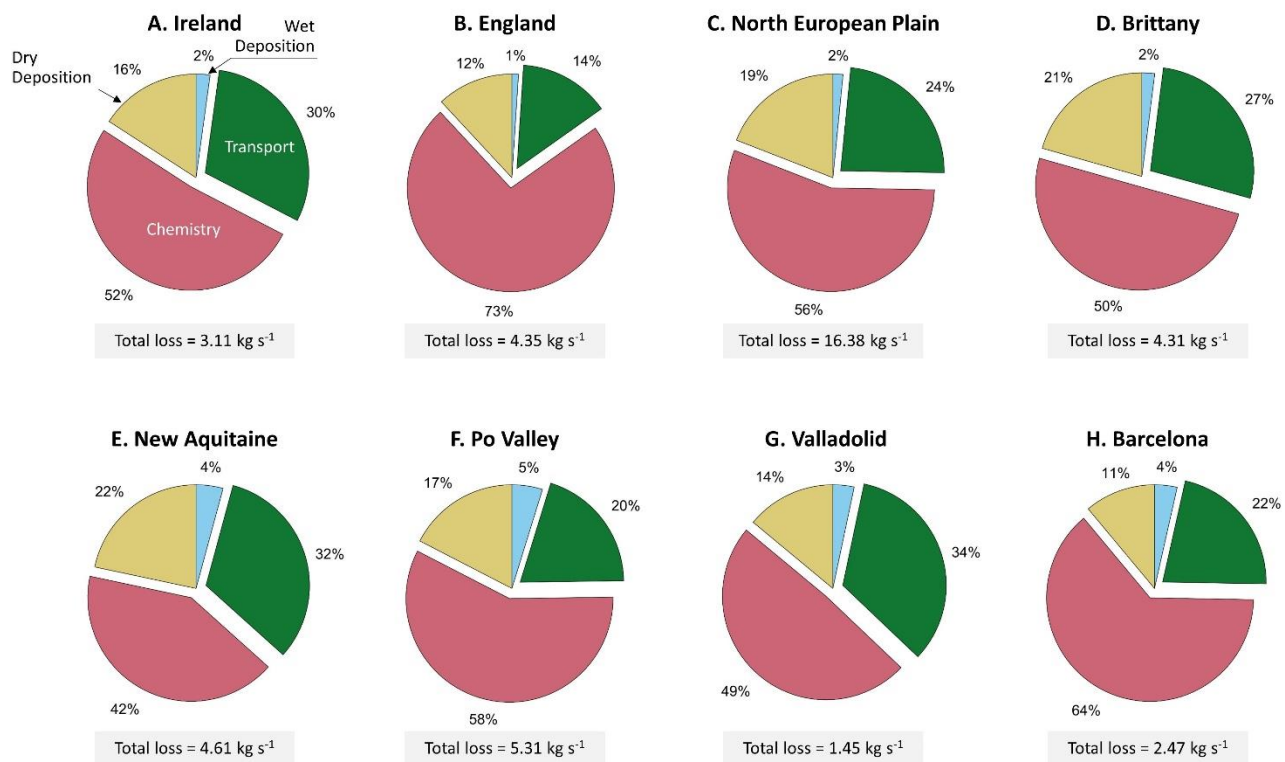
Figure 3. Repartition of the ammonia loss mechanisms for major agricultural areas in Europe, during March 2011, as retrieved from GEOS-Chem, with the total ammonia loss shown in a grey box under each pie chart (kg s⁻¹). The regions are shown in black boxes in Figure 2a.

324 During March, precipitation is relatively lower as compared to winter (December, January, February) in Europe. Furthermore,
325 2011 was a particular dry year compared to the 1981 – 2010 average (Met Office, 2016). Drought was reported to be severe in
326 areas such as France, Belgium and the Netherlands, and moderate in England and Ireland (EDO, 2011). This can help explain
327 the low percentage of wet deposition during March 2011 (1 to 5 % out of the total loss of ammonia).
328

3.2. Ammonia emission potential over Europe

To calculate emission potential, a calculation of the mass transfer coefficient k, which relates to the land type, is necessary. Figure 4 shows the land cover type from MODIS in Europe (left panel), and the corresponding assigned mass transfer coefficient k (right panel) needed to calculate the emission potential (Eq. (2-1)). In order to choose a mass transfer coefficient that is convenient for the different land types relevant to this study, we searched for k values in the literature. Note that ammonia transfer coefficients are not available for all land types.

For water bodies and other land types that are not considered here (see Sect. 2.2), the mass transfer values k were set to zero and represented in grey in Figure 4. In a laboratory experiment, Svensson et al. (1993) reported $k = 4.3 \times 10^{-3}$ m s^{-1} for a mixture of soil and swine manure, therefore, therefore, this value was assigned to croplands. Due to the lack of NH$_3$ k values for non-fertilized forests, shrublands and grasslands in the literature, we used values originally assigned for SO$_2$, bearing in mind that these are approximate values and they reflect mostly the conditions of the soil cover type (short, medium or tall grass) rather than the gas itself. In Aneja et al. (1986), the authors estimated the mass transfer coefficient for both NH$_3$ and SO$_2$ above different types of crops, they found similar values. For NH$_3$, k varied between 0.3 and 1.3 cm s^{-1}, and for SO$_2$ it varied between 0.5 and 1.5 cm s^{-1} (Aneja et al., 1986). Since the latter study estimates several values for NH$_3$ mass transfer coefficient, over different types of crops, we will use the k provided by Svensson et al. (1993), since it is better adapted to reflect NH$_3$ emission from fertilizers, and is not dependent on the crop type. To assign a k value for forests, we used values reported in Aneja (1986) ($k = 2 \times 10^{-2}$ m s^{-1}), which originally represent deposition velocity (mass transfer) of SO$_2$ in a forest (high crops), since both SO$_2$ and NH$_3$ showed similar k in above crops. For shrublands and grasslands (the two land types have the same k), we used the value $k = 8 \times 10^{-3}$ m s^{-1} that has been reported in Aneja et al. (1986) as the deposition velocity (mass transfer) of SO$_2$ in a grassland (medium crops). These values obtained by using MODIS land cover types and published estimates of k values represent our best effort to realistic mass transfer coefficients, and therefore realistic soil emission potentials.

After choosing the k values, we assigned them for each land type on the (500 m $\times$ 500 m) grid. We then aggregate the array with the k values from 500 m $\times$ 500 m to the resolution of GEOS-Chem (0.5° $\times$ 0.625° grid box). This leads to averaging different fine pixels with different land cover types into a coarser grid. The result is shown on the right panel of Figure 4.
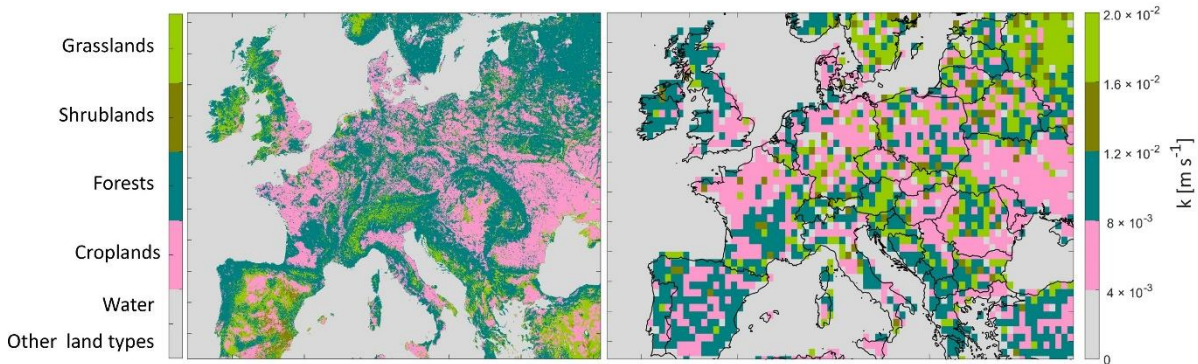
Figure 4. MODIS Land Cover Type, at a 500 m $\times$ 500 m grid box (left panel), and interpolated mass transfer coefficient k (variable k) on a horizontal resolution of 0.5° $\times$ 0.625° grid box (right panel).

Uncertainties of this methodological approach can be summarized as follows:
  (1) The k value assigned for croplands is approximate and therefore not the same in every cropland over Europe.
  (2) The k value assigned for forests represents the SO$_2$ exchange in high croplands; this value may be very different for ammonia, since NH$_3$ can easily dissolve in the water film on leaves under conditions of high humidity.
  (3) While changing the resolution of a fine array (500 m $\times$ 500 m), several grid points are merged and averaged together in order to construct the coarser grid box (0.5° $\times$ 0.625°); the result is therefore an average that might mix croplands with neighboring forests/barelands/grasslands. This leads to a range of different k values that are shown on Figure 4.

365 Using a land-type specific k value is necessary in order to reflect realistic emissions potential, we call this the variable k, as
366 ammonia exchange in a forest is different from that of croplands or unfertilized grasslands, due to different barriers (long,
367 medium or short crop / grass), and ammonium soil content in each land type.
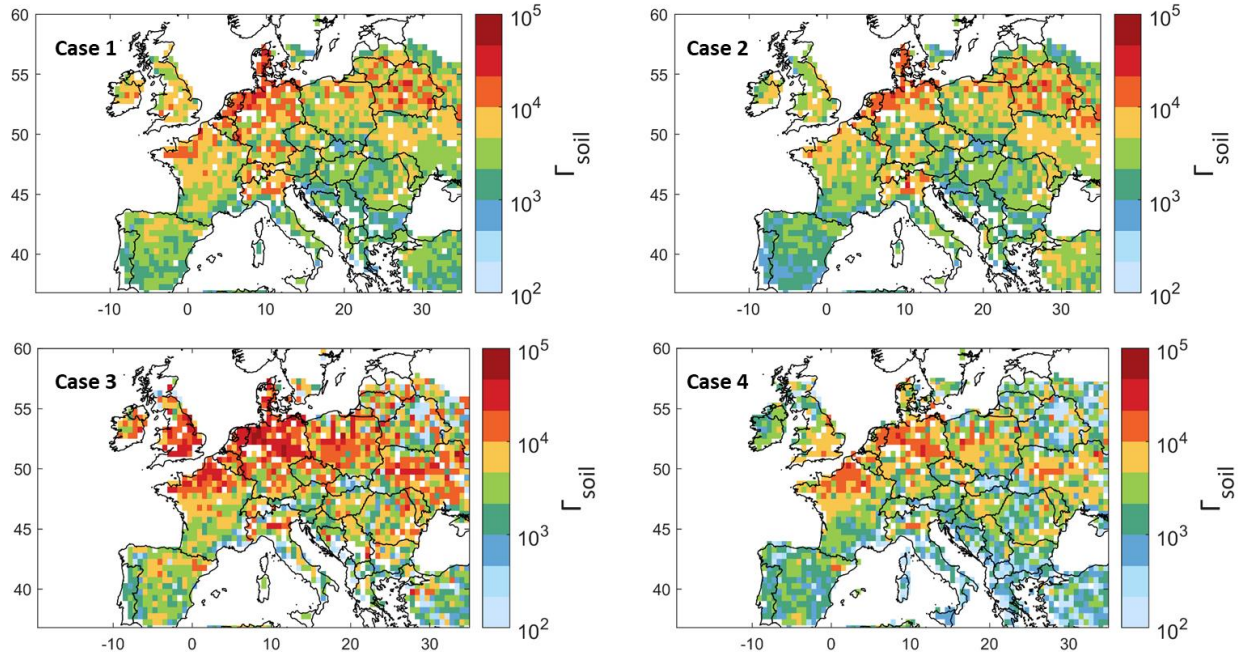
Figure 5. Ammonia soil emission potential (Γ_{soil}) on a log10 scale from model simulation, observation and reanalysis for 4 different cases (see text for details).

368
369 Figure 5 illustrates the ammonia soil emission potential Γ_{soil} calculated using Eq. (2-1) and k values presented in Figure 4.
370 After assigning a variable mass transfer coefficient, the remaining variables needed to calculate Γ_{soil} in Eq. (2-1) are ammonia
371 concentration and lifetime, as well as the skin temperature. Therefore, the emission potential Γ_{soil} shown in Figure 5 is
372 calculated using different configurations:

373
374 - Case 1: GEOS-Chem ammonia and lifetime with MERRA-2 T skin, i.e. simulated Γ_{soil},
375 - Case 2: GEOS-Chem ammonia and lifetime and ERA5 Tskin, to check the effect of using ERA5 vs MERRA-2 for
376 skin temperature,
377 - Case 3: IASI ammonia, ERA5 T skin and GEOS-Chem ammonia lifetime,
378 - Case 4: IASI ammonia, ERA5 T skin and ammonia lifetime from Evangeliou et al. (2021), that were calculated using
379 LMDz-OR-INCA chemistry transport model. The latter couples three models: The general circulation model GCM
380 (LMDz) (Hourdin et al., 2006), the INteraction with Chemistry and Aerosols (INCA) (Folberth et al., 2006), and the
381 land surface dynamical vegetation model (ORCHIDEE) (Krinner et al., 2005).

382
383 We show in supplementary material Figure S2, the emission potential (similarly to what we show in Figure 5) but from a fixed
384 and averaged k value for all land types. Figure S2 shows the importance of using a variable k that is adjusted to each land type
385 is depicted in supplementary materials (Figure S2). To calculated a fixed k (common to all land types) we assume 14 days of
386 fertilization ($k = 10^{-3}$ m s^{-1}, e.g. croplands), 7 days when k value is reducing ($k = 10^{-5}$ m s^{-1}), and 10 days when k is low
387 ($k = 10^{-6}$ m s^{-1}, e.g. forests) resulting in average of $k = 4.5 \times 10^{-4}$ m s^{-1}. The difference in the emission potential between
388 fixed and spatially variable k is shown in supplementary material Figure S3, where we see that a fixed k might overestimate
389 Γ_{soil} by 10 to 10^3 on a log10 scale (500 – 3000 %), in agricultural areas.

390
391 When calculating Γ_{soil}, we filtered data points with ammonia total column concentration less than 5×10^{14} molecules cm^{-2}. The
392 latter are mostly grid boxes concentrated above 56° North that we consider as noise (shown in white pixels on Figure 5).

393

394 T skin from ERA5 and MERRA-2 agree very well, with a coefficient of determination r² = 0.97 (Figure S4 in the supplementary
395 material). This explains the excellent spatial correlation between cases 1 and 2. Note that when using MERRA-2 T skin, we
396 selected only morning measurements from 8:00 to 10:00 UTC. Since IASI-NH₃ retrievals use ERA5 T skin, this also suggests
397 that using MERRA-2 or ERA5 does not affect our Γ_{soil} calculation. In case 3, the emission potential agrees spatially with that
398 of GEOS-Chem. However, we observe higher Γ_{soil} in regions such as Ireland, England, Northern France, Northeastern Spain,
399 and Poland. This is due to the underestimation of ammonia from GEOS-Chem as compared to IASI observations (Figure 1a).
400 For instance, Γ_{soil} from IASI and ERA5 (case 3) differs with that from GEOS-chem and ERA5 (case 1) by 31 % in Ireland.
401 Looking at Table 1, this difference can be explained by the corresponding MRD for Ireland– is −45 %. The differences between
402 case 3 and 4 reach up to +72 % in Ireland, and this is mostly due to the 10-hours difference between ammonia lifetime from
403 GEOS-Chem and Evangeliou et al. (2021) (Figure S1 in the supplementary material). The lowest Γ_{soil} (in most regions) were
404 obtained in case 4, due to the higher lifetime values from Evangeliou et al. (2021), as compared to those calculated from GEOS-
405 Chem (Figure S1); note that Γ_{soil} is inversely proportional to ammonia lifetime (Eq. (2-1). In fact, the longer ammonia stays in
406 the atmosphere (longer lifetime), the less the flux will be directed from the soil to the atmosphere (less ammonia emission).
407 We compared Γ_{soil} calculated from all cases by for each region, and we conclude that cases 2 and 4 showed the best
408 compatibility. For instance, Γ_{soil} from cases 2 and 4 differ by only 6 % in the North European Plain and Brittany, and by 4 %
409 in New Aquitaine. The highest difference between cases 2 and 4 is observed in the Po Valley (53 %) (not shown here).
410 In the four cases presented in Figure 5, we see similar spatial distribution of ammonia emission potential with values ranging
411 from 12×10^{-1} in a forest to 9.5×10^4 in a cropland (monthly average considering all the cases). In agricultural lands, our results
412 show that Γ_{soil} ranges from 2×10^3 to 9.5×10^4. In fact, most of the studies summarized in Zhang et al. (2010) reported Γ_{soil}
413 that range mostly from 10^3 to 10^4 in fertilized croplands/grasslands; the minimum Γ_{soil} reported is in the order of 10^2 and the
414 maximum is of the order of 10^5. Therefore, our values fit within the range of Γ_{soil} calculated in the literature and summarized
415 in Zhang et al. (2010) and the references within. Personne et al. (2015) focused on Grignon, an agricultural region near Paris,
416 France (48∘51′N, 1∘58′E). They obtained Γ_{soil} values between 1.1×10^4 to 5.8×10^6. In the present study, the emission potential
417 over this region is between 4×10^3 (case 2) to 5×10^3 (case 4). In this study, lower values than those measured in the field are
418 expected. Therefore, we consider our results to be in good agreement with the values in Personne et al. (2015), since ours reflect
419 a 31-day mean of an average of over a large area (55×70 km²) as compared to the localized measurements done by Personne
420 et al. (2015).

421

422 The mean emission potentials per ammonia source region in Europe (shown in rectangles in Figure 2 and Figure 3) and per
423 case are shown in Figure 6, and listed in Table 1. Table 1 shows the average lifetime from GEOS-Chem (hours), the average
424 T skin from the two datasets that we used (°C), the average ammonia emission potential in all the cases examined
425 (dimensionless), and the average ammonia columns from IASI and GEOS-Chem (molecules cm⁻²). The four cases show a
426 similar pattern with the North European Plain exhibiting the highest emission potential. This has been shown in Figure 1, Figure
427 2, and Figure 5, as well as in Table 1, where Γ_{soil} is higher in regions with high ammonia columns. This is expected in fertilized
428 lands (croplands), since Γ_{soil} is proportional to the concertation of ammonia near the surface. The latter increases when the soil
429 content of ammonium (NH₄⁺) increases following the application of nitrogen-based fertilizers.

430
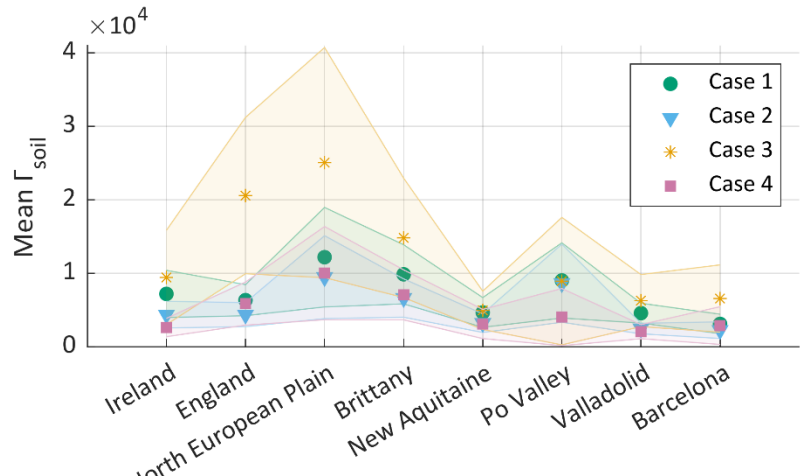
Figure 6. Mean ammonia emission potential Γ_{soil} per region and per case, with the error margin on the mean as the shaded area (95ᵗʰ percentile) for cases 1 to 4. The cases are explained in the discussion of Figure 5.

431   Figure 6 also shows that for cases 1 and 2 (GEOS-Chem) the emission potential in the Po Valley is almost equal to case 3
432   (IASI), with $\Gamma_{soil} = 0.9$ and 0.86×10^4 in cases 1 and 2, and 0.89×10^4 in case 3 (see Table 1). To calculate Γ_{soil} from IASI
433   NH_3 (case 3 and 4), we used T skin from ERA5 that coincides with the overpass of IASI. We used the same T skin values from
434   ERA5 for case 2, as well as hourly concentrations of ammonia from GEOS-Chem (8:30 to 11:30 UTC). The ERA5 T skin are
435   shown in Table 1. The effect of skin temperature through Eq. (2-1) makes the emission potential highly dependent on it. In
436   fact, Γ_{soil} is both directly and inversely proportional to T skin, however, the exponential in the denominator has ~10 times more
437   effect on the value of Γ_{soil} than the T skin in the numerator. Therefore, through Eq. (2-1), we conclude that an increase in
438   temperature by 1°C will reduce Γ_{soil} by around -8 %.
439
440   The standard deviation (shaded area) is found to be the highest in the North European Plain, which is also the largest region
441   (hence higher variability is expected), especially when considering case 3 with IASI. IASI distinguishes different source sub-
442   regions, leading to higher spatial variability of ammonia, and therefore Γ_{soil}.
443

444 **Table 1. Summary of ammonia average lifetime, emission potential, concentrations and the T skin in selected**
445 **regions in Europe.**

446
447
448

Region	Country	τ_{NH_3} [hours]	T skin [°C]		$\Gamma_{soil} \times 10^4$ [dimensionless]				NH₃ concentrations [molecules $\times 10^{15}$ cm⁻²]		
			ERA5 9:30 UTC	MERRA-2 8:00 to 10:00 UTC	Case 1	Case 2	Case 3	Case 4	IASI	GEOS-Chem	Mean MRD [%]
Ireland	Ireland	3.34	8.74	6.23	0.72	0.44	0.94	0.26	2.5	1.4	− 45
England	England	3.15	8.54	5.73	0.63	0.44	2.06	0.58	4.7	1	− 79.2
North European Plain	Belgium, Netherlands	5.16	7.46	4.57	1.22	0.95	2.51	1.00	7.6	3.5	− 55
Brittany	France	6.93	10.48	8.16	0.98	0.66	1.48	0.70	5.8	3.2	− 43.2
New Aquitaine	France	8.05	11.25	7.47	0.46	0.32	0.49	0.30	4.0	2.6	− 34.1
Po Valley	Italy	7.10	8.95	5.46	0.90	0.86	0.89	0.40	4.0	3.8	+ 0.1
Valladolid	Spain	4.53	11.64	6.93	0.46	0.25	0.62	0.20	2.5	1.1	− 57
Barcelona	Spain	4.94	12.61	9.44	0.31	0.25	0.65	0.28	3.2	1.4	− 57.5

449
450
451
452
453
454
455

456
457

     3.3. The effect of temperature change on the volatilization of ammonia

459 As seen in Eq. (2-1), higher skin temperatures favour volatilization of ammonia from the soil. In an attempt to
460 understand how our simplified emission potential model behaves under changing climate, as well as under future
461 scenarios, we adopt the future T skin simulations from EC-Earth climate model, into Eq. (2-1). The two climate
462 socio-economic scenarios that we consider are SSP2-4.5 ("middle of the road" scenario where trends broadly
463 follow their historical patterns), and SSP5-8.5 (a world of rapid and unconstrained growth in economic output and
464 energy use) (Riahi et al., 2017). The same Figure constructed using Γ_{soil} from GEOS-Chem (case 1) is shown in
465 the supplementary material as Figure S5.
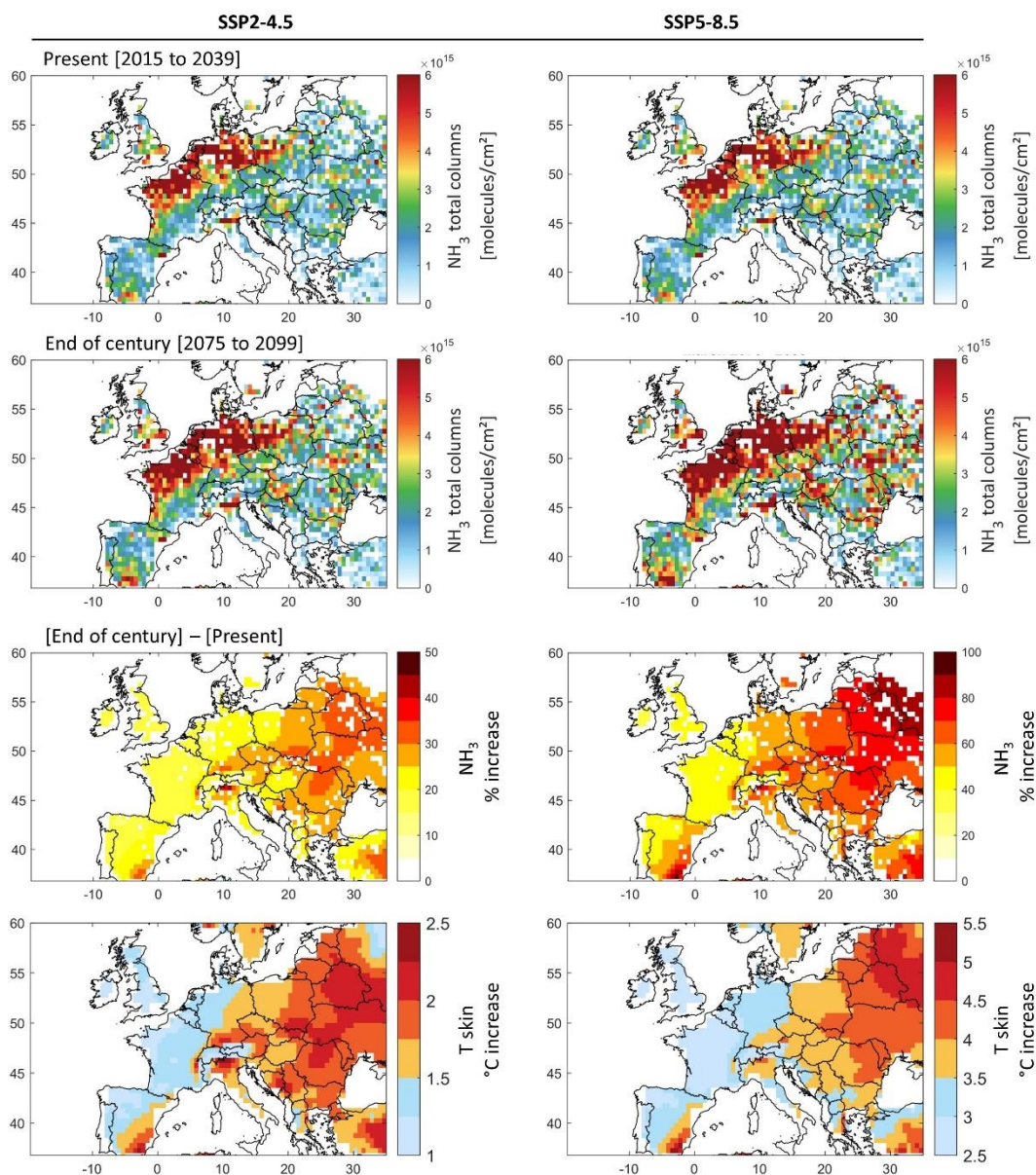
Figure 7. First and second rows: Ammonia total column concentrations during March (monthly averages) under the present climate [2015 to 2039] (first row), and in the end of century climate [2075 to 2099] (second row), under the socio-economic scenarios SSP2-4.5 (left) and SSP5-8.5 (right). Third and fourth rows: The percentage increase in ammonia concentration (third row), and the change in T skin in °C (fourth row) by the end of the century [2075 to 2099] with respect to present climate [2015 to 2039] under SSP2-4.5 (left) and SSP5-8.5 (right). Ammonia columns were calculated using ammonia emission potential Γ_{soil} derived from IASI and ERA5 for March 2011 (case 3), and EC-Earth T skin simulations for SSP2-4.5 and SSP5-8.5 extending from 2015 till 2099.

466 We calculate current and future ammonia columns assuming that the emission potential Γ_{soil} remains unchanged.
467 In other words, we assume that the same amount of fertilizers and manure is used until 2100 in the agricultural
468 fields and farms (unchanged ammonium soil content).

469 Figure 7 shows ammonia columns during the 25-year [2015 – 2039] representing the present climate (upper
470 panels), and the end of the century [2075 – 2099] (middle panels). The ammonia columns in the 25-year average
471 climate of the end of century with respect to present day climate (lower panels) are also shown.
472
473 Spatially, the present climate ammonia columns calculated from the T skin of the climate model and our emission
474 potential from IASI (case 3 in Figure 5), agree very well with those shown in Figure 1. We do not aim at validating
475 or directly comparing the two, as we are only interested in the climate response on ammonia concentration, i.e. by
476 the difference due to skin temperature increase (lower panels).
477
478 From Figure 7 (lower panels) it can be seen that the increase in ammonia columns by the end of the century is
479 more severe in Eastern Europe. Under the most likely scenario (SSP2-4.5), ammonia columns vary between +15
480 % in France, to around +20 % in the North European Plain (Figure 7). The largest increase is detected in Eastern
481 Europe, where ammonia columns show an increase of up to +50 % (Figure 7, lower left panels), creating new
482 potential hotspots/sources of ammonia in Belarus, Ukraine, Hungary, Moldova, parts of Romania and Switzerland.
483 Under the SSP5-8.5 scenario, the results show an increase in ammonia columns of up to +100 % in Eastern Europe
484 (Figure 7, right lower panel). This is directly related to the higher projected increase in skin temperature over these
485 regions. Other studies have equally reported Eastern Europe to be more affected by climate change under future
486 scenarios, as compared to western Europe (European Environment Agency, 2022; Jacob et al., 2018). Spatially,
487 the increase in ammonia coincides with the increase in T skin.
488 Figure 8 depicts the change in ammonia columns under the SSP2-4.5 and SSP5-8.5 scenarios, for our source
489 regions (shown as rectangles in Figure 2). Ammonia columns increase is foreseen to be the highest in the Po Valley
490 (Italy) with +26 % and +59 % under SSP2-4.5 and SSP5-8.5 respectively. It is then followed by the agricultural
491 areas around Barcelona (Spain), and the North European Plain (Belgium, Netherlands) with an increase of +21 %
492 (+49 %) and +20 % (+53 %) respectively, under the SSP2-4.5 (SSP5-8.5) scenario. Under the SSP5-8.5, the
493 increase in ammonia columns in percentage is more than twice the change under SSP2-4.5 (+127 % in the case of
494 the Po Valley for instance). The Po Valley is adjacent to the Alps mountains, and due to global warming, this
495 region is expected to experience increased evapotranspiration (Donnelly et al., 2017), which is a major factor that
496 leads to the volatilization of ammonia.
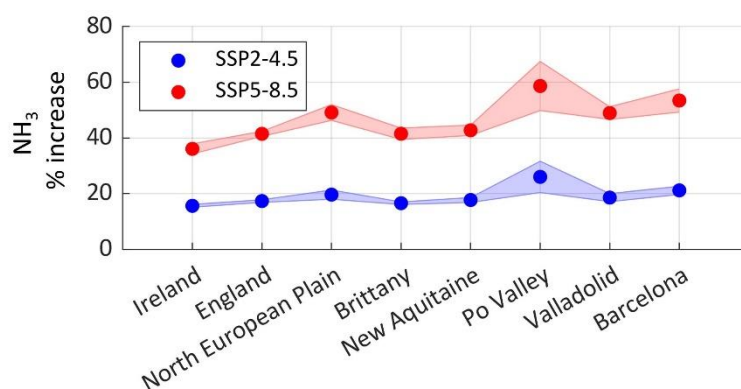
Figure 8. The percentage increase in ammonia concentration by the end of the century [2075 to 2099] with respect to the present climate [2015 to 2039] under the two climate scenarios SSP2-4.5 (blue) and SSP5-8.5 (red), in the source regions investigated in this study. The shades around each line represent the standard deviation from the mean.

497 The local and regional effect of volatilization of ammonia under different climate scenarios remains difficult to be
498 properly assessed. Even under the "middle of the road" scenario 2-4.5, and without climate extremes (e.g.
499 heatwaves), Europe might be facing big challenges in air quality for regions nearby or downwind agricultural
500 regions, since chemistry and atmospheric transport (Figure 3) drive the loss of ammonia during the growing season
501 in this part of the world.
502
503 An increase in ammonia concentration poses a significant and yet poorly understood effect on local and regional
504 air quality through the increase in $PM_{2.5}$ concentration. We note, however, that ammonia columns in the soil are
505 governed by a threshold. Higher temperatures will increase the rate of volatilization of ammonia from the soil, but
506 only up to a certain point where no dissolved ammonium is left. Plants, however, can also be a source of ammonia
507 when exposed to stressful conditions. For example, under heat stress and in instances where there is no ammonia
508 in the air, increase in air temperature results in exponential increase in ammonia emission from plants' leaves
509 (Husted and Schjoerring, 1996).

4. Conclusions

Agriculture worldwide has fed the human race for thousands of years, and will continue to do so, as mankind highly relies on it. Emissions from agricultural activities will inevitably increase, in order to meet the expected yield. In this study, we use a variety of state-of-the-art datasets (satellite, reanalysis and model simulation) to calculate the first regional map of ammonia emission potential during the start of the growing season in Europe. The emission potential can be used as a proxy to calculate ammonia columns in the atmosphere, and as such to assess its deposition, atmospheric transport, and contribution to PM formation. First, we show that the GEOS-Chem chemistry transport model is able to reproduce key spatio-temporal patterns of ammonia levels over Europe. The ammonia budget is governed by the emissions over source regions (North European Plain, Brittany and the Po valley), as well as by key loss processes. We find that chemical loss pathway is responsible of 50 % or more of the total ammonia loss over Europe. From the GEOS-Chem simulation, we calculate the average ammonia lifetime in the atmosphere which ranges between 4 and 12 hours in agricultural source regions of Europe. From this, and using the mass transfer coefficient for different land cover types, we calculate a range of emission potentials Γ_{soil} from IASI and GEOS-Chem. We find that Γ_{soil} ranges between from 0.2×10^4 to 2.5×10^4 in fertilized lands (croplands). Choosing a variable k from the literature, and based on different land cover types from MODIS, we calculate Γ_{soil} values that are consistent with those found in the literature. The increase in T skin is expected to have an effect on the emission of ammonia from the soil. Using T skin from the EC-Earth climate model, we estimate ammonia columns by the end of the century [2075 – 2099], and compare it to columns of the present climate [2015 – 2039]. Our results show that ammonia columns might double under the SSP5-8.5 scenario, and might increase by up to 50 % under the most likely SSP2-4.5 scenario. The eastern part of Europe is the most affected by the change in temperatures, and it is where we find the highest ammonia columns increase. Among the regions of focus, Italy, Spain, Belgium and the Netherlands are the most affected, as compared to France, England and Ireland. The highest increase in ammonia columns is observed in the Po Valley in Italy (+59 % under the SSP5-8.5).

We calculate ammonia concentration under future climate and during the start of the growing season (March) in Europe. However, in order to grasp the yearly budget of ammonia, it is crucial to apply this method to all seasons of the year; especially in regions with extensive agricultural activities, such as the United States, India, and China. In addition to this, more field measurements of ammonia emission potential (Γ_{soil}) in different land use / cover types are required, this can help us perform better comparison with emission potentials calculated from model and satellite data. Finally, having ammonia columns at different times of the day, from field observations or satellite measurements will allow quantification of daily emission potentials, that will in turn help us understand its diurnal variability. This will be ensured with the launch of the Infrared Sounder (IRS) on the Meteosat Third Generation (MTG) geostationary satellites scheduled in 2025.

A. Appendix A

1. Ammonia-Ammonium equilibrium

Ammonia (NH_3) is a water-soluble gas, it undergoes protonation with H^+ from the hydronium ion H_3O^+ in an aqueous solution in order to give ammonium (NH_4^+ cation), the dissociation equation is expressed as follows:

$$NH_{3\,(aq)} + H_3O^+ \xoverleftrightarrow{K_{NH4+}} NH_{4\,(aq)}^+ + HO^- \tag{A-1}$$

Or
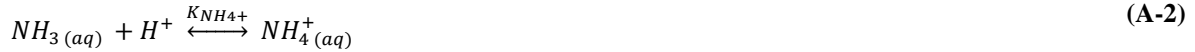
$$NH_{3\,(aq)} + H^+ \xoverleftrightarrow{K_{NH4+}} NH_{4\,(aq)}^+ \tag{A-2}$$

With K_{NH4+} as the ammonium-ammonia dissociation equilibrium constant that can be expressed as:

$$K_{NH_4^+} = \frac{[NH_{3\,(aq)}][H^+]}{[NH_{4\,(aq)}^+]} \tag{A-3}$$

The solubility of ammonia in water is affected by the temperature and the acidity (pH) of the solvent (water). The equilibrium constant can be expressed as follows:

$$K_{NH_4+} = 5.67 \cdot 10^{-10} \exp\left[-6286 \left(\tfrac{1}{T} - \tfrac{1}{298.15}\right)\right] \tag{A-4}$$

2. Henry's equilibrium

Upon its dissolution in water, NH_3 obeys the Henry's law. Ammonia gas ($NH_{3\,(g)}$) near the surface of the solvent is in equilibrium with the dissolved ammonia in the aqueous phase $NH_{3\,(aq)}$ (in water). Henry's equilibrium is expressed as follows:
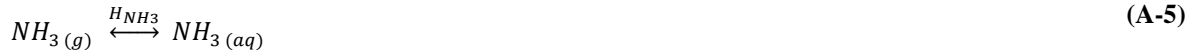
$$NH_{3\,(g)} \xoverleftrightarrow{H_{NH3}} NH_{3\,(aq)} \tag{A-5}$$

where H_{NH3} is Henry's constant, which can be expressed as follows (Wichink Kruit, 2010):

$$H_{NH3} = \frac{[NH_{3\,(aq)}]}{[NH_{3\,(g)}]} = 5.527 \cdot 10^{-4} \cdot \exp\left[4092 \left(\tfrac{1}{T} - \tfrac{1}{298.15}\right)\right] \tag{A-6}$$

The partial pressure of ammonia near the surface of the soil can be calculated using Henry's constant and the dissociation equilibrium (Wichink Kruit, 2010):

$$P_{NH3} = \frac{K_{NH_4^+}\,[NH_4^+]}{H_{NH3}\,[H^+]} = \frac{5.67 \cdot 10^{-10} \cdot \exp\left[-6286\left(\tfrac{1}{T}-\tfrac{1}{298.15}\right)\right]}{5.527 \cdot 10^{-4} \cdot \exp\left[4092\left(\tfrac{1}{T}-\tfrac{1}{298.15}\right)\right]} \times \frac{[NH_4^+]}{[H^+]} \tag{A-7}$$

If we use the ideal gas law (PV=nRT), we can draw the link between the mass density of ammonia ($NH_{3\,(g)}$) and the partial pressure:

$$\chi_{NH_3} = \frac{P_{NH_3} \cdot M_{NH_3}}{R \cdot T} \tag{A-8}$$

Where χ_{NH_3} is the concentration of NH_3 at the soil surface (kg m^{-3}), P_{NH3} is the partial pressure of NH_3 near the surface (atm), M_{NH3} is the molar mass of NH_3 (kg mol^{-1}), R is the gas constant (0.082 atm L mol^{-1} K^{-1}), and T is the temperature in Kelvin.
Substituting Eq. (A-7) into (A-8) we get:

$$\chi_{NH_3} = \frac{2.75 \cdot 10^9 \left(\tfrac{gK}{m^3}\right)}{T_{soil}} \exp\left[\frac{-1.04 \cdot 10^4}{T_{soil}}\right] \Gamma_{soil} \tag{A-9}$$

Where χ_{NH_3} is the concentration of ammonia at the soil surface at equilibrium (g m^{-3}), and is referred to as the compensation point, T_{soil} is the temperature of the soil (Kelvin), Γ_{NH_3} is the NH_3 emission potential from the soil and is a dimensionless ratio between [NH_4^+] and [H^+].

3. Ammonia total columns from IASI

In this study we use the total columns of ammonia from IASI (molecules m^{-2}) since in order to calculate the emission potential Γ_{soil}, we should draw the link between these columns and this parameter. The bi-directional exchange of NH$_3$ between the surface and the atmosphere can be expressed by the flux (assuming a flux independent of time) (Roelle and Aneja, 2005; Zhang et al., 2010):

$$Flux_{NH_3} = k \, ([NH_3]^{soil} - [NH_3]^{atm}) \tag{A-10}$$

where $Flux_{NH_3}$ is the bidirectional flux between the soil and the atmosphere (molecules (m² s)$^{-1}$), k is the soil – atmosphere exchange velocity (m s^{-1}), also known as the mass transfer coefficient; $[NH_3]^{soil}$ is the concentration of NH$_{3(g)}$ in the soil, and $[NH_3]^{atm}$ is the concentration of NH$_{3(g)}$ in the atmosphere near the surface (molecules m^{-3}). We can consider that $[NH_3]^{atm}$ is identical to the total column of NH$_3$ provided by IASI and denoted here as $[NH_3]^{col}$. This is because most of the atmospheric NH$_3$ are located in the lower boundary layer (Dammers et al., 2019).Assuming a first order dissociation of NH$_3$, we can express the change in the $[NH_3]^{col}$ total columns as follows:

$$\frac{d \, [NH_3]^{col}}{dt} = Flux_{NH_3} - k'[NH_3]^{col} \tag{A-11}$$

Where k' is the rate of dissociation of first order $k' = 1/\tau$ (m s^{-1}), with τ the lifetime of NH$_3$ in the atmosphere. Assuming steady state, and considering the $[NH_3]^{atm}$ as the $[NH_3]^{col}$, and $[NH_3]^{soil}$ as χ_{NH_3}, Eq. (A-11) can be written as:

$$k \left(\frac{N_a \cdot \chi_{NH_3}}{M_{NH_3}} - \frac{1}{c} \, [NH_3]^{col} \right) = \frac{[NH_3]^{col}}{\tau} \tag{A-12}$$

Where c is the column height and is equal to 6 km. It is important to note that we neglect the effect of transport by wind since we only look at large regions. Finally, the total column of ammonia $[NH_3]^{col}$ can be written as:

$$[NH_3]^{col} = \frac{N_a \cdot \chi_{NH_3}}{M_{NH_3} \cdot (c + \frac{1}{k\tau})} \tag{A-13}$$

The column height is not considered anymore because it is negligible compared to $1/_{k\tau}$, using Eq. (A-9) into (A-13) we get:

$$[NH_3]^{col} = \frac{2.75 \cdot 10^{27}\left(\frac{gK}{cm^3}\right)}{T_{soil}} \exp\left[\frac{-1.04 \cdot 10^4}{T_{soil}}\right] \Gamma_{NH_3} \cdot k\tau \qquad \left(\frac{molecules}{cm^2}\right) \tag{A-14}$$

Note that $2.75 \cdot 10^{27} = \frac{a \cdot N_a \cdot c'}{M_{NH_3}} \left(\frac{K \, molecules}{cm^3}\right)$, where $a = 2.75 \cdot 10^3 \, (g \, K \, cm^{-3})$, N_a Avogadro's number (6.0221409 $\times 10^{23}$ molecules mol^{-1}), 10^{-2} is added to convert k from m s^{-1} to cm s^{-1}, and M_{NH_3} the molar mass of NH$_3$ (17.031 g mol^{-1}). The emission potential of NH$_3$ from the soil can we written as:

$$\Gamma_{soil} = \frac{[NH_3]^{col} \cdot T_{soil}}{\exp(\frac{-b}{T_{soil}})} \frac{M_{NH_3}}{a \cdot N_a \cdot 10^{-2}} \cdot \frac{1}{k\tau} \tag{A-15}$$

where $b = 1.04 \times 10^4 \, K$.

Author contribution

RA contributed to the conception and design of the article, developed the code, wrote the manuscript, analysed and interpreted of the data, and approved the version for submission; CV, CC, and PFC revised the manuscript; WCP provided the GEOS-Chem simulation data, and revised the manuscript; NE provided ammonia lifetime calculation using the LMDz-OR-INCA chemistry transport model and commented on the manuscript; MVD and LC contributed to the acquisition of the IASI ammonia data (NH3-v3R-ERA5), and revised the manuscript; SS contributed to the conception and design of the article, provided the EC-Earth temperature data, and revised the manuscript, and approved the version for submission.

Acknowledgments

The IASI mission is a joint mission of Eumetsat and the Centre National d'Etudes Spatiales (CNES, France). The authors acknowledge the Aeris data infrastructure for providing the IASI L1C and L2 data.

Funding information

Rimal Abeed is grateful to CNES for financial support. The research in Belgium was funded by the Belgian State Federal Office for Scientific, Technical and Cultural Affairs (Prodex HIRS) and the Air Liquide Foundation (TAPIR project). This work is also partly supported by the FED-tWIN project ARENBERG ("Assessing the Reactive Nitrogen Budget and Emissions at Regional and Global Scales") funded via the Belgian Science Policy Office (BELSPO). L. Clarisse is Research Associate supported by the Belgian F.R.S.-FNRS. C. Clerbaux is grateful to CNES for scientific collaboration and financial support. N. Evangeliou was funded by Norges Forskningsråd (ROM- FORSK – Program for romforskning of the Research Council of Norway (grant no. 275407)).

Competing interests

The authors are aware of no competing interests.

Data accessibility statement

The IASI-NH$_3$ used in this study are retrieved from the Aeris data infrastructure (https://iasi.aeris-data.fr/nh3r-era5/). ERA5 skin temperature from 1979 to present are available for download in the following DOI: 10.24381/cds.adbb2d47. The GEOS-Chem outputs used in this study are only available upon request. EC-Earth3 model output prepared for CMIP6 ScenarioMIP are retrieved here: https://doi.org/10.22033/ESGF/CMIP6.727. The MODIS land cover data are available for download in the following link: https://doi.org/10.5067/MODIS/MCD12Q1.006.

References

Abeed, R., Clerbaux, C., Clarisse, L., Van Damme, M., Coheur, P.-F., and Safieddine, S. A space view of agricultural and industrial changes during the Syrian civil war. *Elem. Sci. Anthr.* https://doi.org/10.1525/elementa.2021.000041 (2021)

Adams, C., McLinden, C. A., Shephard, M. W., Dickson, N., Dammers, E., Chen, J., Makar, P., Cady-Pereira, K. E., Tam, N., Kharol, S. K., Lamsal, L. N., and Krotkov, N. A. Satellite-derived emissions of carbon monoxide, ammonia, and nitrogen dioxide from the 2016 Horse River wildfire in the Fort McMurray area. *Atmospheric Chem. Phys.* https://doi.org/10.5194/acp-19-2577-2019 (2019)

Agreste. (2014). *Enquête Pratiques culturales 2011—Grandes cultures et prairies | Agreste, la statistique agricole* (No. 21; Agreste Les Dossiers). Ministère de l'Agriculture, de l'Agroalimentaire et de la Forêt. https://agreste.agriculture.gouv.fr/agreste-web/disaron/dos21/detail/

Alexander, B., Sherwen, T., Holmes, C. D., Fisher, J. A., Chen, Q., Evans, M. J., and Kasibhatla, P. Global inorganic nitrate production mechanisms: Comparison of a global model with nitrate isotope observations. *Atmospheric Chem. Phys.* https://doi.org/10.5194/acp-20-3859-2020 (2020)

Aneja, V. P., Rogers, H. H., and Stahel, E. P. Dry Deposition of Ammonia at Environmental Concentrations on Selected Plant Species. *J. Air Pollut. Control Assoc.* https://doi.org/10.1080/00022470.1986.10466183 (1986)

AQEG. *Fine particulate matter (PM2.5) in the United Kingdom* (p. 203). Air Quality Expert Group (AQEG), prepared for the Department for Environment, Food and Rural Affairs (Defra), Scottish Executive, Welsh Government and the Department of the Environment in Northern Ireland. https://uk-air.defra.gov.uk/assets/documents/reports/cat11/1212141150_AQEG_Fine_Particulate_Matter_in_the_UK.pdf (2012)

Barnes, A. P., Svensson, C., and Kjeldsen, T. R. North Atlantic air pressure and temperature conditions associated with heavy rainfall in Great Britain. *Int. J. Climatol.* https://doi.org/10.1002/joc.7414 (2022)

Bauer, S. E., Tsigaridis, K., and Miller, R. Significant atmospheric aerosol pollution caused by world food cultivation. *Geophys. Res. Lett.* https://doi.org/10.1002/2016GL068354 (2016)

Behera, S. N., Sharma, M., Aneja, V. P., and Balasubramanian, R. Ammonia in the atmosphere: A review on emission sources, atmospheric chemistry and deposition on terrestrial bodies. *Env. Sci Pollut Res.* https://doi.org/10.1007/s11356-013-2051-9 (2013)

Belward, A. S., Estes, John E., and Kline, K. D. The IGBP-DIS Global 1-Km Land-Cover Data Set DIS-Cover: A Project Overview. *Photogramm. Eng. Remote Sens.* https://www.asprs.org/wp-content/uploads/pers/1999journal/sep/1999_sept_1013-1020.pdf (1999)

Bey, I., Jacob, D. J., Yantosca, R. M., Logan, J. A., Field, B. D., Fiore, A. M., Li, Q., Liu, H. Y., Mickley, L. J., and Schultz, M. G. Global modeling of tropospheric chemistry with assimilated meteorology: Model description and evaluation. *J. Geophys. Res. Atmospheres.* https://doi.org/10.1029/2001JD000807 (2001)

Bouwman, A. F., Lee, D. S., Asman, W. a. H., Dentener, F. J., Van Der Hoek, K. W., and Olivier, J. G. J. A global high-resolution emission inventory for ammonia. *Glob. Biogeochem. Cycles.* https://doi.org/10.1029/97GB02266 (1997)

Clarisse, L., Van Damme, M., Clerbaux, C., and Coheur, P.-F. Tracking down global NH3 point sources with wind-adjusted superresolution. *Atmospheric Meas. Tech.* https://doi.org/10.5194/amt-12-5457-2019 (2019)

Clarisse, L., Van Damme, M., Gardner, W., Coheur, P.-F., Clerbaux, C., Whitburn, S., Hadji-Lazaro, J., and Hurtmans, D. Atmospheric ammonia (NH3) emanations from Lake Natron's saline mudflats. *Sci. Rep.* https://doi.org/10.1038/s41598-019-39935-3 (2019)

Clerbaux, C., Boynard, A., Clarisse, L., George, M., Hadji-Lazaro, J., Herbin, H., Hurtmans, D., Pommier, M., Razavi, A., Turquety, S., and Wespes, C. Monitoring of atmospheric composition using the thermal infrared IASI/MetOp sounder. *Atmospheric Chem. Phys.* https://doi.org/10.5194/acp-9-6041-2009 (2009)

Coheur, P.-F., Clarisse, L., Turquety, S., Hurtmans, D., and Clerbaux, C. IASI measurements of reactive trace species in biomass burning plumes. *Atmospheric Chem. Phys.* https://doi.org/10.5194/acp-9-5655-2009 (2009)

Dammers, E., McLinden, C. A., Griffin, D., Shephard, M. W., Van Der Graaf, S., Lutsch, E., Schaap, M., Gainairu-Matz, Y., Fioletov, V., Van Damme, M., Whitburn, S., Clarisse, L., Cady-Pereira, K., Clerbaux, C., Coheur, P. F., and Erisman, J. W. NH₃ emissions from large point sources derived from CrIS and IASI satellite observations. *Atmospheric Chem. Phys.* https://doi.org/10.5194/acp-19-12261-2019 (2019)

David, M., Loubet, B., Cellier, P., Mattsson, M., Schjoerring, J. K., Nemitz, E., Roche, R., Riedo, M., and Sutton, M. A. Ammonia sources and sinks in an intensively managed grassland canopy. *Biogeosciences*. https://doi.org/10.5194/bg-6-1903-2009 (2009)

Donnelly, C., Greuell, W., Andersson, J., Gerten, D., Pisacane, G., Roudier, P., and Ludwig, F. Impacts of climate change on European hydrology at 1.5, 2 and 3 degrees mean global warming above preindustrial level. *Clim. Change*. https://doi.org/10.1007/s10584-017-1971-7 (2017)

Döscher, R., Acosta, M., Alessandri, A., Anthoni, P., Arneth, A., Arsouze, T., Bergmann, T., Bernadello, R., Bousetta, S., Caron, L.-P., Carver, G., Castrillo, M., Catalano, F., Cvijanovic, I., Davini, P., Dekker, E., Doblas-Reyes, F. J., Docquier, D., Echevarria, P., … Zhang, Q. The EC-Earth3 Earth System Model for the Climate Model Intercomparison Project 6. *Geosci. Model Dev. Discuss.* https://doi.org/10.5194/gmd-2020-446 (2021)

ECMWF. *IFS Documentation CY43R1*. ECMWF. https://www.ecmwf.int/sites/default/files/elibrary/2016/17117-part-iv-physical-processes.pdf (2016)

EDO, G. D. O. *Drought news in Europe: Situation in April 2011—Short Analysis of data from the European Drought Observatory (EDO)* (p. 2). https://edo.jrc.ec.europa.eu/documents/news/EDODroughtNews201104.pdf (2011)

Einarsson, R., Sanz-Cobena, A., Aguilera, E., Billen, G., Garnier, J., van Grinsven, H. J. M., & Lassaletta, L. (2021). Crop production and nitrogen use in European cropland and grassland 1961–2019. *Scientific Data*, *8*(1), Article 1. https://doi.org/10.1038/s41597-021-01061-z

Erisman, J. W., Van Pul, A., and Wyers, P. Parametrization of surface resistance for the quantification of atmospheric deposition of acidifying pollutants and ozone. *Atmos. Environ.* https://doi.org/10.1016/1352-2310(94)90433-2 (1994)

European Environment Agency. *Nitrogen Dioxide (NO₂): annual mean concentrations in Europe*. https://www.eea.europa.eu/themes/air/interactive/no2 (2017a)

European Environment Agency. *Sulphur Dioxide (SO₂): annual mean concentrations in Europe*. https://www.eea.europa.eu/themes/air/interactive/so2 (2017b)

European Environment Agency. *Global and European temperatures*. https://www.eea.europa.eu/ims/global-and-european-temperatures (2022)

Evangeliou, N., Balkanski, Y., Eckhardt, S., Cozic, A., Van Damme, M., Coheur, P.-F., Clarisse, L., Shephard, M., Cady-Pereira, K., and Hauglustaine, D. 10-year satellite-constrained fluxes of ammonia improve performance of chemistry transport models. *Atmospheric Chem. Phys.* https://doi.org/10.5194/acp-21-4431-2021 (2021)

Eyring, V., Bony, S., Meehl, G. A., Senior, C. A., Stevens, B., Stouffer, R. J., and Taylor, K. E. Overview of the Coupled Model Intercomparison Project Phase 6 (CMIP6) experimental design and organization. *Geosci. Model Dev.* https://doi.org/10.5194/gmd-9-1937-2016 (2016)

FAO. *FAO, GIEWS, Earth Observation*. https://www.fao.org/giews/earthobservation/country/index.jsp?lang=enandcode=FRA (2022)

Fertilizers Europe. *Infinite Fertilizers—Nutrient Stewardship*. https://www.fertilizerseurope.com/wp-content/uploads/2019/08/Nutrient_Stewardship_Sept_2016_websize.pdf. (2016)Flechard, C. R., Massad, R.-S., Loubet, B., Personne, E., Simpson, D., Bash, J. O., Cooter, E. J., Nemitz, E., and Sutton, M. A. Advances in understanding, models and parameterizations of biosphere-atmosphere ammonia exchange. *Biogeosciences*. https://doi.org/10.5194/bg-10-5183-2013 (2013)

Flechard, C. R., Nemitz, E., Smith, R. I., Fowler, D., Vermeulen, A. T., Bleeker, A., Erisman, J. W., Simpson, D., Zhang, L., Tang, Y. S., and Sutton, M. A. Dry deposition of reactive nitrogen to European ecosystems: A comparison of inferential models across the NitroEurope network. *Atmospheric Chem. Phys.* https://doi.org/10.5194/acp-11-2703-2011 (2011)

Flechard, C. R., Spirig, C., Neftel, A., and Ammann, C. The annual ammonia budget of fertilised cut grassland – Part 2: Seasonal variations and compensation point modeling. *Biogeosciences*. https://doi.org/10.5194/bg-7-537-2010 (2010)

Folberth, G. A., Hauglustaine, D. A., Lathière, J., and Brocheton, F. Interactive chemistry in the Laboratoire de Météorologie Dynamique general circulation model: Model description and impact analysis of biogenic hydrocarbons on tropospheric chemistry. *Atmospheric Chem. Phys.* https://doi.org/10.5194/acp-6-2273-2006 (2006)

Garrido-Perez, J. M., Ordóñez, C., García-Herrera, R., and Barriopedro, D. Air stagnation in Europe: Spatiotemporal variability and impact on air quality. *Sci. Total Environ.* https://doi.org/10.1016/j.scitotenv.2018.07.238 (2018)

Gelaro, R., McCarty, W., Suárez, M. J., Todling, R., Molod, A., Takacs, L., Randles, C. A., Darmenov, A., Bosilovich, M. G., Reichle, R., Wargan, K., Coy, L., Cullather, R., Draper, C., Akella, S., Buchard, V., Conaty, A., Silva, A. M. da, Gu, W., … Zhao, B. The Modern-Era Retrospective Analysis for Research and Applications, Version 2 (MERRA-2). *J. Clim.* https://doi.org/10.1175/JCLI-D-16-0758.1 (2017)

Hersbach, H., Bell, B., Berrisford, P., Hirahara, S., Horányi, A., Muñoz-Sabater, J., Nicolas, J., Peubey, C., Radu, R., Schepers, D., Simmons, A., Soci, C., Abdalla, S., Abellan, X., Balsamo, G., Bechtold, P., Biavati, G., Bidlot, J., Bonavita, M., … Thépaut, J.-N. The ERA5 global reanalysis. *Q. J. R. Meteorol. Soc.* https://doi.org/10.1002/qj.3803 (2020)

Hoesly, R. M., Smith, S. J., Feng, L., Klimont, Z., Janssens-Maenhout, G., Pitkanen, T., Seibert, J. J., Vu, L., Andres, R. J., Bolt, R. M., Bond, T. C., Dawidowski, L., Kholod, N., Kurokawa, J., Li, M., Liu, L., Lu, Z., Moura, M. C. P., O'Rourke, P. R., and Zhang, Q. Historical (1750–2014) anthropogenic emissions of reactive gases and aerosols from the Community Emissions Data System (CEDS). *Geosci. Model Dev.* https://doi.org/10.5194/gmd-11-369-2018 (2018)

Hourdin, F., Musat, I., Bony, S., Braconnot, P., Codron, F., Dufresne, J.-L., Fairhead, L., Filiberti, M.-A., Friedlingstein, P., Grandpeix, J.-Y., Krinner, G., LeVan, P., Li, Z.-X., and Lott, F. The LMDZ4 general circulation model: Climate performance and sensitivity to parametrized physics with emphasis on tropical convection. *Clim. Dyn.* https://doi.org/10.1007/s00382-006-0158-0 (2006)

Husted, S., and Schjoerring, J. K. Ammonia Flux between Oilseed Rape Plants and the Atmosphere in Response to Changes in Leaf Temperature, Light Intensity, and Air Humidity (Interactions with Leaf Conductance and Apoplastic $NH4+$ and $H+$ Concentrations). *Plant Physiol.* https://doi.org/10.1104/pp.112.1.67 (1996)

Jacob, D., Kotova, L., Teichmann, C., Sobolowski, S. P., Vautard, R., Donnelly, C., Koutroulis, A. G., Grillakis, M. G., Tsanis, I. K., Damm, A., Sakalli, A., and van Vliet, M. T. H. Climate Impacts in Europe Under +1.5°C Global Warming. *Earths Future*. https://doi.org/10.1002/2017EF000710 (2018)

Keller, C. A., Long, M. S., Yantosca, R. M., Da Silva, A. M., Pawson, S., and Jacob, D. J. HEMCO v1.0: A versatile, ESMF-compliant component for calculating emissions in atmospheric models. *Geosci. Model Dev.* https://doi.org/10.5194/gmd-7-1409-2014 (2014)

Klaes, K. D. The EUMETSAT Polar System. *Comprehensive Remote Sensing*. Elsevier. https://doi.org/10.1016/B978-0-12-409548-9.10318-5 (2018)

Krinner, G., Viovy, N., de Noblet-Ducoudré, N., Ogée, J., Polcher, J., Friedlingstein, P., Ciais, P., Sitch, S., and Prentice, I. C. A dynamic global vegetation model for studies of the coupled atmosphere-biosphere system. *Glob. Biogeochem. Cycles*. https://doi.org/10.1029/2003GB002199 (2005)

Lee, W., An, S., and Choi, Y. Ammonia harvesting via membrane gas extraction at moderately alkaline pH: A step toward net-profitable nitrogen recovery from domestic wastewater. *Chem. Eng. J.* https://doi.org/10.1016/j.cej.2020.126662 (2020)

Lentze, G. *Metop-A satellite retiring after 15 years of huge benefits to forecasting* [Text]. *ECMWF*. ECMWF. https://www.ecmwf.int/en/about/media-centre/news/2021/metop-satellite-retiring-after-15-years-huge-benefits-forecasting (2021, November 12)

Luo, Z., Zhang, Y., Chen, W., Van Damme, M., Coheur, P.-F., and Clarisse, L. Estimating global ammonia (NH_3) emissions based on IASI observations from 2008 to 2018. *Atmospheric Chem. Phys.* https://doi.org/10.5194/acp-22-10375-2022 (2022)

Massad, R.-S., Nemitz, E., and Sutton, M. A. Review and parameterisation of bi-directional ammonia exchange between vegetation and the atmosphere. *Atmospheric Chem. Phys.* https://doi.org/10.5194/acp-10-10359-2010 (2010)

Masson-Delmotte, V., P. Zhai, A. Pirani, S.L., Connors, C. Péan, S. Berger, N. Caud, Y. Chen, L. Goldfarb, M.I. Gomis, M. Huang, K. Leitzell, E. Lonnoy, J.B.R., and Matthews, T.K. Maycock, T. Waterfield, O. Yelekçi, R. Yu, and B. Zhou. *IPCC, 2021: Climate Change 2021: The Physical Science Basis. Contribution of Working Group I to the Sixth Assessment Report of the Intergovernmental Panel on Climate Change*. Cambridge University Press. In Press. https://www.ipcc.ch/assessment-report/ar6/ (2021)

Mattsson, M., B, H., M, D., Loubet, B., M, R., Theobald, M., Sutton, M., Bruhn, D., Neftel, A., and Schjoerring, J. Temporal variability in bioassays of ammonia emission potential in relation to plant and soil N parameters in intensively managed grassland. *Biogeosciences Discuss.* https://doi.org/10.5194/bgd-5-2749-2008 (2008)

McDuffie, E. E., Smith, S. J., O'Rourke, P., Tibrewal, K., Venkataraman, C., Marais, E. A., Zheng, B., Crippa, M., Brauer, M., and Martin, R. V. A global anthropogenic emission inventory of atmospheric pollutants from sector- and fuel-specific sources (1970–2017): An application of the Community Emissions Data System (CEDS). *Earth Syst. Sci. Data*. https://doi.org/10.5194/essd-12-3413-2020 (2020)

Met Office. *Exceptionally warm and dry Spring 2011*. Met Office. https://www.metoffice.gov.uk/binaries/content/assets/metofficegovuk/pdf/weather/learn-about/uk-past-events/interesting/2011/exceptionally-warm-and-dry-spring-2011---met-office.pdf (2016)

Nemitz, E., Sutton, M. A., Schjoerring, J. K., Husted, S., and Paul Wyers, G. Resistance modelling of ammonia exchange over oilseed rape. *Agric. For. Meteorol.* https://doi.org/10.1016/S0168-1923(00)00206-9 (2000)

Olesen, J. E., and Sommer, S. G. Modelling effects of wind speed and surface cover on ammonia volatilization from stored pig slurry. *Atmospheric Environ. Part Gen. Top.* https://doi.org/10.1016/0960-1686(93)90030-3 (1993)

Personne, E., Tardy, F., Génermont, S., Decuq, C., Gueudet, J.-C., Mascher, N., Durand, B., Masson, S., Lauransot, M., Fléchard, C., Burkhardt, J., and Loubet, B. Investigating sources and sinks for ammonia exchanges between the atmosphere and a wheat canopy following slurry application with trailing hose. *Agric. For. Meteorol.* https://doi.org/10.1016/j.agrformet.2015.03.002 (2015)

Phillips, S. B., Arya, S. P., and Aneja, V. P. Ammonia flux and dry deposition velocity from near-surface concentration gradient measurements over a grass surface in North Carolina. *Atmos. Environ.* https://doi.org/10.1016/j.atmosenv.2004.02.054 (2004)

Pinder, R. W., Gilliland, A. B., and Dennis, R. L. Environmental impact of atmospheric NH3 emissions under present and future conditions in the eastern United States. *Geophys. Res. Lett.* https://doi.org/10.1029/2008GL033732 (2008)

Plumb, R. A., and Stolarski, R. S. Chapter 2: The Theory of Estimating Lifetimes Using Models and Observations. *SPARC Lifetimes Rep. 2013 – SPARC Rep. No 6*. https://pages.jh.edu/rstolar1/other_pubs/LifetimeReport_Ch2.pdf (2013)

Potapov, P., Turubanova, S., Hansen, M. C., Tyukavina, A., Zalles, V., Khan, A., Song, X.-P., Pickens, A., Shen, Q., and Cortez, J. Global maps of cropland extent and change show accelerated cropland expansion in the twenty-first century. *Nat. Food*. https://doi.org/10.1038/s43016-021-00429-z (2022)

Randerson, J. T., Van Der Werf, G. R., Giglio, L., Collatz, G. J., and Kasibhatla, P. S. Global Fire Emissions Database, Version 4.1 (GFEDv4). *ORNL DAAC*. https://doi.org/10.3334/ORNLDAAC/1293 (2015)

Riahi, K., van Vuuren, D. P., Kriegler, E., Edmonds, J., O'Neill, B. C., Fujimori, S., Bauer, N., Calvin, K., Dellink, R., Fricko, O., Lutz, W., Popp, A., Cuaresma, J. C., Kc, S., Leimbach, M., Jiang, L., Kram, T., Rao, S., Emmerling, J., … Tavoni, M. The Shared Socioeconomic Pathways and their energy, land use, and greenhouse gas emissions implications: An overview. *Glob. Environ. Change*. https://doi.org/10.1016/j.gloenvcha.2016.05.009 (2017)

Roelle, P. A., and Aneja, V. P. Modeling of Ammonia Emissions from Soils. *Environ. Eng. Sci.* https://doi.org/10.1089/ees.2005.22.58 (2005)

Schlesinger, W. H., and Hartley, A. E. A global budget for atmospheric NH3. *Biogeochemistry*. https://doi.org/10.1007/BF00002936 (1992)

Shen, H., Chen, Y., Hu, Y., Ran, L., Lam, S. K., Pavur, G. K., Zhou, F., Pleim, J. E., and Russell, A. G. Intense Warming Will Significantly Increase Cropland Ammonia Volatilization Threatening Food Security and Ecosystem Health. *One Earth*. https://doi.org/10.1016/j.oneear.2020.06.015 (2020)

Shephard, M. W., and Cady-Pereira, K. E. Cross-track Infrared Sounder (CrIS) satellite observations of tropospheric ammonia. *Atmos Meas Tech*. https://doi.org/10.5194/amt-8-1323-2015 (2015)

Sulla-Menashe, D., and Friedl, M. A. *User Guide to Collection 6 MODIS Land Cover (MCD12Q1 and MCD12C1) Product*. https://lpdaac.usgs.gov/documents/101/MCD12_User_Guide_V6.pdf (2018)

Svensson, L., and Ferm, M. Mass Transfer Coefficient and Equilibrium Concentration as Key Factors in a New Approach to Estimate Ammonia Emission from Livestock Manure. *J. Agric. Eng. Res.* https://doi.org/10.1006/jaer.1993.1056 (1993)

Theobald, M. R., Crittenden, P. D., Hunt, A. P., Tang, Y. S., Dragosits, U., and Sutton, M. A. Ammonia emissions from a Cape fur seal colony, Cape Cross, Namibia. *Geophys. Res. Lett.* https://doi.org/10.1029/2005GL024384 (2006)

Tournadre, B., Chelin, P., Ray, M., Cuesta, J., Kutzner, R. D., Landsheere, X., Fortems-Cheiney, A., Flaud, J.-M., Hase, F., Blumenstock, T., Orphal, J., Viatte, C., and Camy-Peyret, C. Atmospheric ammonia (NH$_3$ over the Paris megacity: 9 years of total column observations from ground-based infrared remote sensing. *Atmospheric Meas. Tech.* https://doi.org/10.5194/amt-13-3923-2020 (2020)

USDA. *Europe—Crop Calendars. Foreign Agric. Serv. US Dep. Agric.* Foreign Agricultural Service, U.S. Department of Agriculture. https://ipad.fas.usda.gov/rssiws/al/crop_calendar/europe.aspx (2022, May 12)

Van Damme, M., Clarisse, L., Franco, B., Sutton, M. A., Erisman, J. W., Wichink Kruit, R., van Zanten, M., Whitburn, S., Hadji-Lazaro, J., Hurtmans, D., Clerbaux, C., and Coheur, P.-F. Global, regional and national trends of atmospheric ammonia derived from a decadal (2008-2018) satellite record. *Environ. Res. Lett.* https://doi.org/10.1088/1748-9326/abd5e0 (2021)

Van Damme, M., Clarisse, L., Whitburn, S., Hadji-Lazaro, J., Hurtmans, D., Clerbaux, C., and Coheur, P.-F. Industrial and agricultural ammonia point sources exposed. *Nature.* https://doi.org/10.1038/s41586-018-0747-1 (2018)

Van Damme, M., Whitburn, S., Clarisse, L., Clerbaux, C., Hurtmans, D., and Coheur, P.-F. Version 2 of the IASI NH3 neural network retrieval algorithm; near-real time and reanalysed datasets. *Atmos. Meas. Tech.,* 10, 4905–4914, https://doi.org/10.5194/amt-10-4905-2017 (2017)

Van Der Molen, J., Beljaars, A. C. M., Chardon, W. J., Jury, W. A., and Faassen, H. G. van. Ammonia volatilization from arable land after application of cattle slurry. 2. Derivation of a transfer model. *Neth. J. Agric. Sci.* https://doi.org/10.18174/njas.v38i3A.16586 (1990)

Viatte, C., Abeed, R., Yamanouchi, S., Porter, W., Safieddine, S., Van Damme, M., Clarisse, L., Herrera, B., Grutter, M., Coheur, P.-F., Strong, K., and Clerbaux, C. NH$_3$ spatio-temporal variability over Paris, Mexico and Toronto and its link to PM$_{2.5}$ during pollution events. *EGUsphere.* https://doi.org/10.5194/egusphere-2022-413 (2022)

Viatte, C., Petit, J.-E., Yamanouchi, S., Van Damme, M., Doucerain, C., Germain-Piaulenne, E., Gros, V., Favez, O., Clarisse, L., Coheur, P.-F., Strong, K., and Clerbaux, C. Ammonia and PM2.5 Air Pollution in Paris during the 2020 COVID Lockdown. *Atmosphere.* https://doi.org/10.3390/atmos12020160 (2021)

Viatte, C., Wang, T., Van Damme, M., Dammers, E., Meleux, F., Clarisse, L., Shephard, M. W., Whitburn, S., Coheur, P. F., Cady-Pereira, K. E., and Clerbaux, C. Atmospheric ammonia variability and link with particulate matter formation: A case study over the Paris area. *Atmospheric Chem. Phys.* https://doi.org/10.5194/acp-20-577-2020 (2020)

Wentworth, G. R., Murphy, J. G., Gregoire, P. K., Cheyne, C. A. L., Tevlin, A. G., and Hems, R. Soil–atmosphere exchange of ammonia in a non-fertilized grassland: Measured emission potentials and inferred fluxes. *Biogeosciences.* https://doi.org/10.5194/bg-11-5675-2014 (2014)

Wesely, M. L. Parameterization of surface resistances to gaseous dry deposition in regional-scale numerical models. *Atmospheric Environ. 1967.* https://doi.org/10.1016/0004-6981(89)90153-4 (1989)

Whitburn, S., Damme, M. V., Clarisse, L., Bauduin, S., Heald, C. L., Hadji-Lazaro, J., Hurtmans, D., Zondlo, M. A., Clerbaux, C., and Coheur, P.-F. A flexible and robust neural network IASI-NH3 retrieval algorithm. *J. Geophys. Res. Atmospheres.* https://doi.org/10.1002/2016JD024828 (2016)

Wichink Kruit, R. Surface-atmosphere exchange of ammonia. Ph.D., Wageningen University. Wageningen, Netherlands, https://edepot.wur.nl/137586 (2010)

Yang, S., Yuan, B., Peng, Y., Huang, S., Chen, W., Hu, W., Pei, C., Zhou, J., Parrish, D. D., Wang, W., He, X., Cheng, C., Li, X.-B., Yang, X., Song, Y., Wang, H., Qi, J., Wang, B., Wang, C., … Shao, M. The formation and mitigation of nitrate pollution: Comparison between urban and suburban environments. *Atmospheric Chem. Phys.* https://doi.org/10.5194/acp-22-4539-2022 (2022)

Yu, F., Nair, A. A., and Luo, G. Long-Term Trend of Gaseous Ammonia Over the United States: Modeling and Comparison with Observations. *J. Geophys. Res. Atmospheres.* https://doi.org/10.1029/2018JD028412 (2018)

Zhang, L., Wright, L. P., and Asman, W. a. H. Bi-directional air-surface exchange of atmospheric ammonia: A review of measurements and a development of a big-leaf model for applications in regional-scale air-quality models. *J. Geophys. Res. Atmospheres*. https://doi.org/10.1029/2009JD013589 (2010)